Arabian Journal of Geosciences (2023) 16:471
https://doi.org/10.1007/s12517-023-11586-9

ORIGINAL PAPER

Orogenic exhumation, erosion, and sedimentation in a pro-foreland basin: central Pindos foreland basin, western Greece

Chrysanthos Botziolis[1] · Angelos G. Maravelis[2] · George Pantopoulos[3] · Ioannis Iliopoulos[4] · George Iliopoulos[5] · Avraam Zelilidis[1]

Received: 20 April 2023 / Accepted: 30 June 2023 / Published online: 14 July 2023

Abstract

In western Greece is the Pindos Foreland Basin, a geological depression that contains approximately 2500 m of mainly Upper Eocene to Lower Oligocene submarine fans deposits. Despite the extensive stratigraphic and structural research that has defined the basin as a foreland basin that developed adjacent to Pindos Orogen, the impact of orogenic history and erosion on sedimentation has not been evaluated. This study investigates the origin and tectonic setting of the central Pindos Foreland Basin using new provenance data. Petrographic and geochemical analyses suggest that the succession was primarily sourced by sedimentary, felsic, and intermediate igneous, and low-grade metamorphic source rocks. The geochemical analysis reveals that the sediments are immature and have undergone little to moderate weathering, and low degrees of sediment recycling and sorting. A secondary mafic source with high Cr and Ni contents and high Cr/V ratios. The provenance data indicate that Pindos Orogen represents the source region and agree with the existing sedimentological and palaeocurrent research. The Pindos sedimentary and Pelagonian volcano-sedimentary units, mixed with a mafic source (Pindos ophiolitic units) and low grade metamorphics produce the observed chemical and petrographic variance. Multidimensional discrimination diagrams suggest sediment sources from a collisional setting and confirm the active continental edge setting. The provenance data display an up-section increase in lithic fragments, recording the growing history of the Pindos orogen and the gradual exhumation of the source regions. This study offers an example of the sedimentary provenance trend in an evolving pro foreland basin.

Keywords Foreland basin · Sub-marine fans · Provenance · Pindos Orogen · Unroofing · Eocene-Oligocene

Introduction

Collisional orogens and associated sedimentary basins are of great scientific and economic significance because they track information about the collisional processes, refining the geodynamic models, and are related to economically viable resources (Ding et al. 2005; Weislogel et al. 2006; Najman et al. 2010; Maravelis et al. 2012; Nance et al. 2014; Hu et al. 2015; Bega 2015; Velić et al. 2015; Critelli 2018; Tserolas et al. 2019; Critelli and Martín-Martín 2022). Foreland basins are developed in each side of the orogen (in the pro- and retro side) and result from lithosphere flexure, caused by the enormous mass produced by crustal thickening associated with mountain belt development (Beaumont 1981; Sinclair and Allen 1992; Garzanti et al. 2007; Catuneanu 2018; Critelli and Criniti 2021). Further, local factors like basement tectonics and relative eustacy of sea level have an influence on subsidence (Catuneanu 2018). The sedimentary successions in foreland basins provide insights about the growing

Responsible Editor: Attila Ciner

✉ Chrysanthos Botziolis
cbotziolis@upnet.gr

1 Department of Geology, Laboratory of Sedimentology, University of Patras, 26504 Patras, Greece

2 Department of Geology, Aristotle University of Thessaloniki, 54124 Thessaloniki, Greece

3 Department of Earth Sciences "Ardito Desio", University of Milan, 20133 Milan, Italy

4 Department of Geology, Laboratory of Rocks and Minerals Research, University of Patras, 26504 Patras, Greece

5 Department of Geology, Laboratory of Palaeontology and Stratigraphy, University of Patras, 26504 Patras, Greece

and development of orogens and adjacent depocenters (White et al. 2002; Garzanti et al. 2004a, 2004b; Garzanti et al. 2005). These attributes can be further evaluated by using sedimentary and sequence stratigraphic data (Cantalamessa and Di Celma 2004; Catuneanu 2004; Martins-Neto and Catuneanu 2010; Maravelis et al. 2018; Melehan et al. 2021), geochemical (Verma and Armstrong-Altrin 2013; Zaid and Gahtani 2015; Tawfik et al. 2017; Maravelis et al. 2021) and structural data (Ryan and Williams 2007; Maravelis et al. 2017). Processes, such as orogenic unroofing, recycling and erosion can be also investigated by studying the provenance of the detritus that comprise the sedimentary fill in foreland basins. The sedimentary provenance in the two foreland basins (pro- and retro foreland basin) reflects the orogenic evolutionary stages, with the pro foreland displaying an up-section increase in lithic rock fragments, and the retro foreland exhibiting an up-section increase in metamorphic rock fragments (Dorsey 1988; Chen et al. 2001; Kirstein et al. 2009; Nagel et al. 2014; Critelli and Criniti 2021).

Reconstructions of tectonic and paleogeographic history are benefited by provenance investigations that consider the petrographic and geochemical composition of clastic deposits. Petroleum and geochemical studies have identified fundamental elements influencing sediment composition in depositional systems such as climate, drainage system, source-rock composition, and basin geometry (Johnsson 1993; Critelli et al. 2003; Garzanti et al. 2007). Petrographic and geochemistry analyses are effective tools in the study of basin provenance and tectonic setting because sediment composition is directly impacted by transportation processes, source rock composition, tectonic and paleoclimatic conditions of the source area (Zimmermann and Spalletti 2009; Ghazi and Mountney 2011; Garzanti et al. 2013; Maravelis et al. 2015; Fathy et al. 2018; Iqbal et al. 2019). Source rocks for sedimentary successions are identified based on the relative immobility of elements under various tectonic settings, such that their concentration reflects their original composition. Because these components (trace and rare earth elements) are thought to be immobile and inactive while in transit, they are suitable proxies for provenance research (Von-Eynatten et al. 2003).

The examined succession consists of Upper Eocene to Lower Oligocene sub-marine fan deposits. These sedimentary rocks deposited in the central Pindos Foreland Basin (PFB, Fig. 1) are described primarily in terms of sedimentology-stratigraphy that includes lithofacies and depositional environment (Piper et al. 1978; Pavlopoulos 1983; Avramidis and Zelilidis 2001; Botziolis et al. 2021; Kovani et al. 2023; and references therein), structural deformation (Faupl et al. 1998; Kamberis et al. 2000; Sotiropoulos et al. 2003; Piper 2006; Konstantopoulos and Zelilidis 2012; and references therein) and oil-gas potential (Karakitsios and Rigakis 1996; Zelilidis et al. 2003; Zelilidis and Maravelis 2015; and references therein). This work presents an integration of geochemical and petrographic results that further constrain the origin and tectonic setting of these deposits, emphasizing to sedimentary processes, such as weathering, sorting, and recycling that affected the deposition of the central PFB strata. This research elaborates provenance data to link sediment composition to particular stratigraphic units of Pindos orogen, and to highlight the impact of orogenic growth on the sedimentation of Pindos foreland basin.

Geological setting

The complicated geotectonic evolution of western Greece was caused by changes in the type and relative movements of the main tectonic plates. Pindos Orogen (Fig. 1) is a thrust system that separates external from internal Hellenides and is the result of the collision of Apulian and Pelagonian continental blocks, after the closure of Pindos Ocean (De Graciansky et al. 1989; Doutsos et al. 1993, 2006; Karakitsios 2013; Zelilidis et al. 2015).

The sedimentological-stratigraphic and structural assessments of the external Hellinides indicate different evolutionary phases that can be broadly defined as an early extensional and a latter collisional phase (Fig. 2) (Karakitsios 1990, 1995, 2013; Zelilidis et al. 2015; Bourli et al. 2019a, 2019b; Zoumpouli et al. 2022). The early phase is characterized by deposition of carbonates in an extensional setting (Ionian Basin), whereas the sedimentation in the latter phase is dominated by clastics in a foreland basin (PFB). The early pre-rift stage that predates tectonic processes is testified by Lower to Middle Triassic evaporites and Upper Triassic to Lower Jurassic shallow marine limestones (Fig. 2). This stage is followed by the syn-rift stage, during which the sedimentation is represented by late Lower Jurassic to Lower Cretaceous carbonates (with a few rare mudstone successions) with a general deepening upwards sedimentation (Fig. 2). During this stage, syn-sedimentary extensional tectonics develop half-grabens and result in notable thickness fluctuations of the syn-rift deposits (Zelilidis et al. 2015; Bourli et al. 2019a, 2019b). The sedimentation in the final syn-rift stage includes carbonates from the Middle Cretaceous to Lower Eocene (Bourli et al. 2019a, 2019b; Fig. 2).

In western Greece, the Middle Eocene marks the transition from crustal stretching to crustal shortening (Lutetian to Bartonian, Zoumpouli et al. 2022). The Pindos orogen developed because of this plate motion, and it is defined as an elevated plug with both a pro- and a retro-wedge domain in the idea of a doubly vergent thrust wedge (Doutsos et al. 2006). The Pindos orogen suture zone is characterized by ophiolitic rocks (remnants of the former oceanic crust) in the orogen central sections (Robertson 2004). Progradation occurred over Triassic evaporites representing the

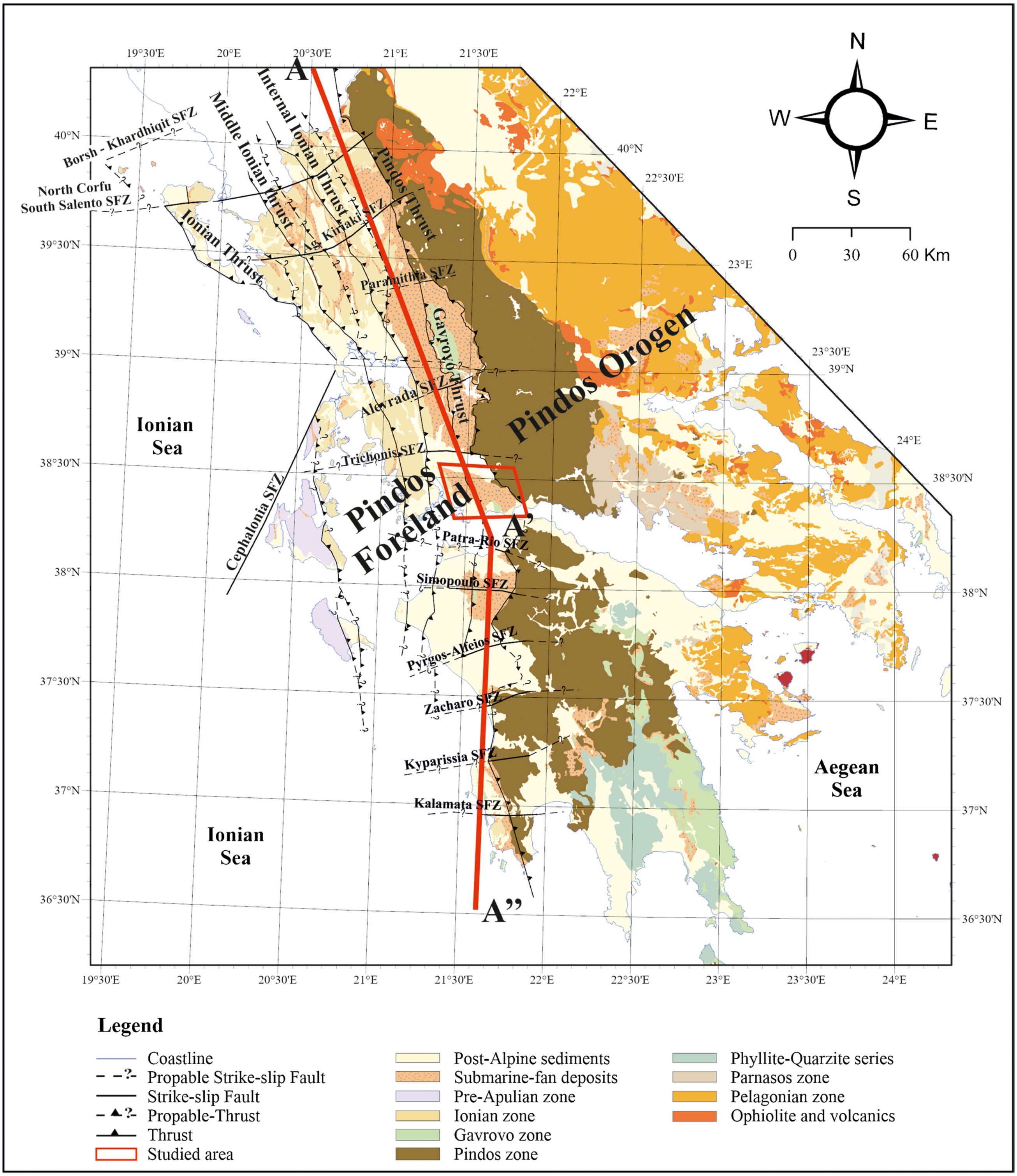

Fig. 1 Geological map of Western Greece (modified from Zelilidis et al. 2015), illustrating the major thrusts and strike-slip fault zones. The red box shows the study area and the profile at the A-A'-A" cross section refers to the schematic diagram of Fig. 19

preferential décollement zone, as evidenced by their proximity to thrusts (Underhill 1988; Karakitsios 1995; Kamberis et al. 1996). The Mesozoic to Eocene carbonate thrust tip anticlines were formed by many intrabasinal thrusts that impacted the basin in the Late Oligocene and Early Miocene (Jenkins 1972; Clews 1989).

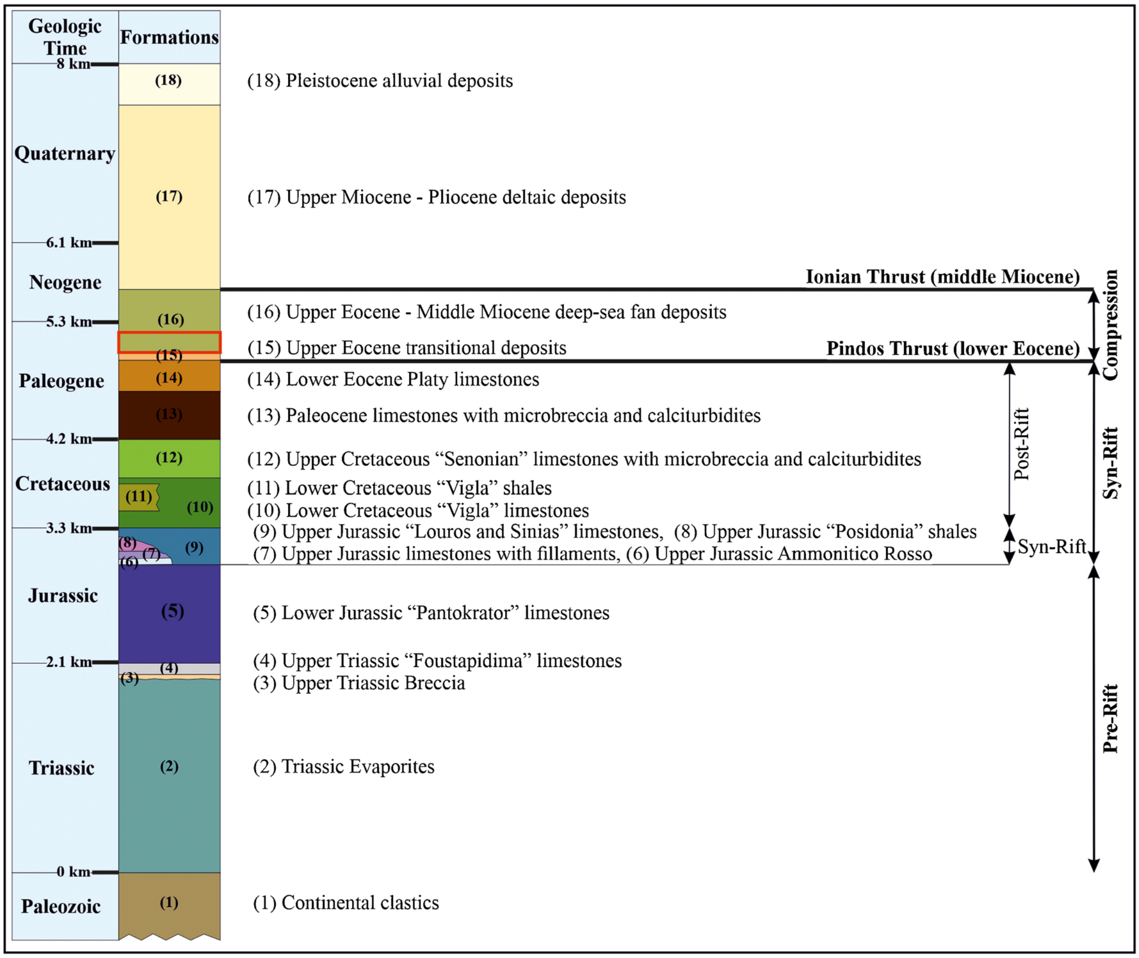

Fig. 2 Lithostratigraphic column of the Ionian zone (modified after Bourli et al. 2019a and Zoumpouli et al. 2022)

The western section of the external Hellenides underwent compression from the Middle Eocene to the Early Miocene (Fig. 2), whereas the eastern section is dominated by extensional tectonics (Aubouin 1959; Jacobshagen 1986; Pavlides et al. 1995; Doutsos and Koukouvelas 1998; Doutsos et al. 2000). Throughout the Late Eocene to Early Oligocene, deep-sea fan sediments were deposited westward in the PFB as a result of the tectonic uplift and erosion of the Pindos orogen (Koch and Nicolaus 1969; Skourlis and Doutsos 2003; Sotiropoulos et al. 2003; Botziolis et al. 2021), evolving up-section to deltaic and alluvial deposits (Fig. 2) (Avramidis and Zelilidis 2001; Piper 2006; Piper et al. 1978; Konstantopoulos and Zelilidis 2012; Botziolis et al. 2021).

The PFB trends parallel to the Pindos orogen and is bounded by the Pindos and the Ionian thrust to the east and the west, respectively (Fig. 1) (Aubouin 1959). The activity of the Pindos thrust was more important during the evolution of the PFB, compared to the Gavrovo, internal Ionian and middle Ionian thrusts (Avramidis et al. 2000). Additionally, and despite the absence of precise chronologic information, structural features, such as thrust-related fault bend and fault progradation folds, as well as the absence of growth strata, suggest that these thrusts postdate the sediment deposition (Zygouri et al. 2021). PFB has also been affected by strike-slip faults (King et al. 1993; Avramidis et al. 2000; Avramidis and Zelilidis 2001; Konstantopoulos et al. 2013). The Pindos thrust is cut by strike-slip faults that operated independently in several locations and epochs, namely in Ioannina in the Early Eocene, Arta in the Late Eocene, and Mesolongi in the Early Oligocene (Fig. 1) (Zelilidis et al. 2008). The strike-slip faults acted as pathways, affected the paleocurrent system, causing sediment to discharge at far-off locations (Zelilidis et al. 2008).

Stratigraphy of Pindos foreland basin

PFB is thought to have formed as a foredeep during the Late Eocene to Early Oligocene, receiving sediments from the rising Pindos Orogen. The investigated succession consists of ten facies and sub-facies associations and thirteen sedimentary facies, according to Botziolis et al. (2021). Central PFB deposits can be divided into three distinct depositional environments (Botziolis et al. 2021; Figs. 3, 4, 5). The study area consists of a submarine fan system overlying Eocene carbonates (Fig. 5a). There is a general trend from west to east from the carbonates, through the abyssal plain (Fig. 5b), to the outer (Fig. 5c), and inner (Fig. 5d) fan deposits, testifying system progradation and temporal shallowing of the PFB (Botziolis et al. 2021). Between the enclosing topography of the levees, conglomeratic channel-belt facies consisting of limestone, chert, sandstone, and shale clasts may be discovered. The sediments were deposited within the Pindos foredeep and belong to the system underfilled stage. The examination of the sediments reveals deposition during the onset of the Pindos orogen, when sedimentation was constrained by the accommodation space provided by lithospheric flexure (Botziolis et al. 2021).

Data from sole markings show two distinct directional flows. Across the stratigraphic strata of the examined sections, the NE-SW orientation of the measurements suggests that the axial flow pattern predominated during sediment deposition (Fig. 4) (Botziolis et al. 2021). Additionally, a flow-spread tendency has been linked to all perpendicular flows and associated with (distal) lobe-fringe or levee deposits. The relationship between space accommodation and sediment transport volume on a subsiding tectonic setting is shown to be essential in shaping subsurface architecture and the subsequent stacking pattern. These controls can be detected by the system geometry and architecture. PFB lobe complexes were developed in an unconfined environment and are distinguished by a compensating stacking pattern, resulting in widespread deposits (Botziolis et al. 2021). This is because of the availability of sufficient space for compensation and a sediment supply insufficient to exceed the accommodation space.

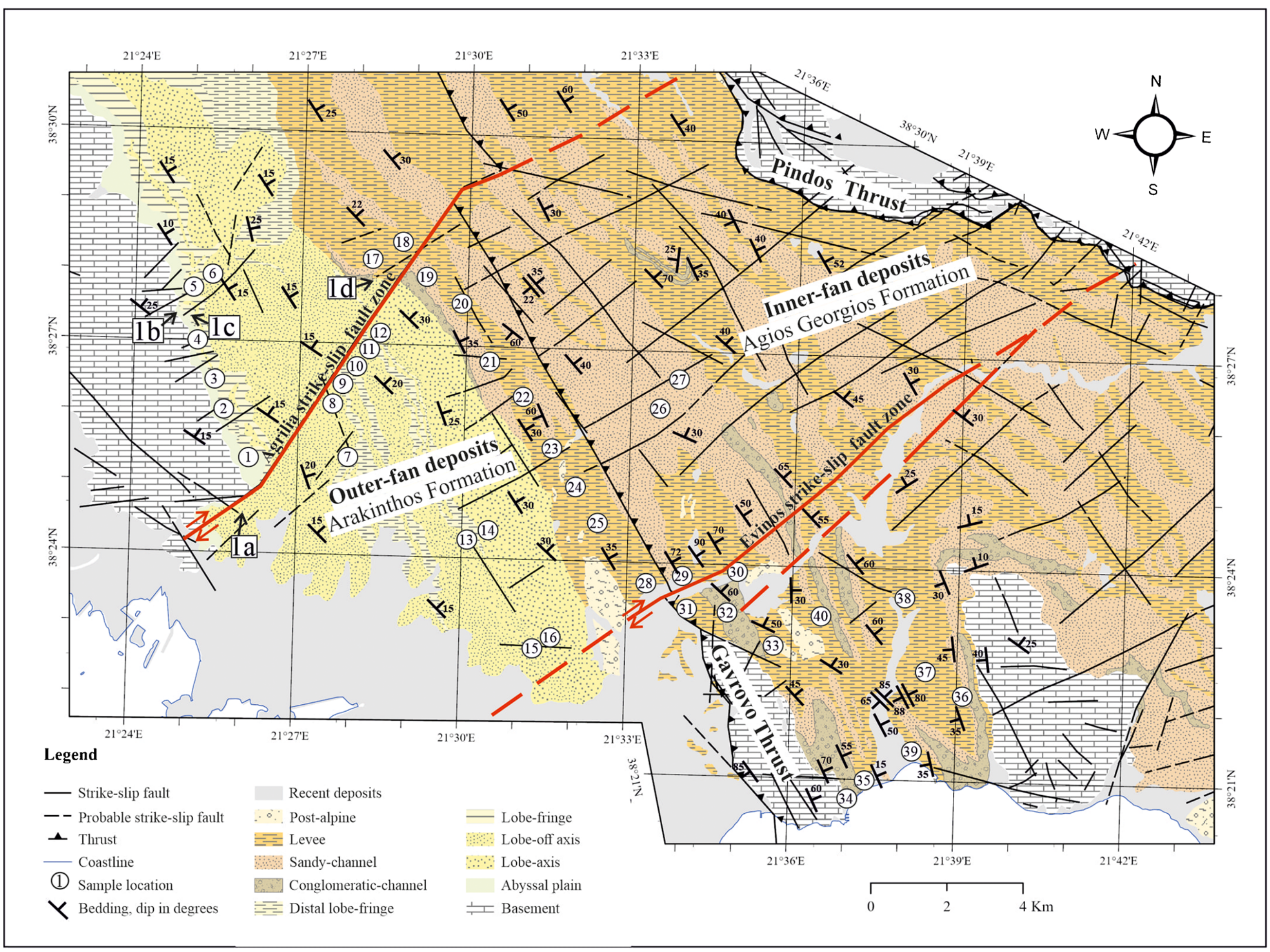

Fig. 3 Geological map of the studied area depicting the analysed outcrops as well as the spatial distribution of the various environments and sub-environments of deposition (modified by Botziolis et al. 2021)

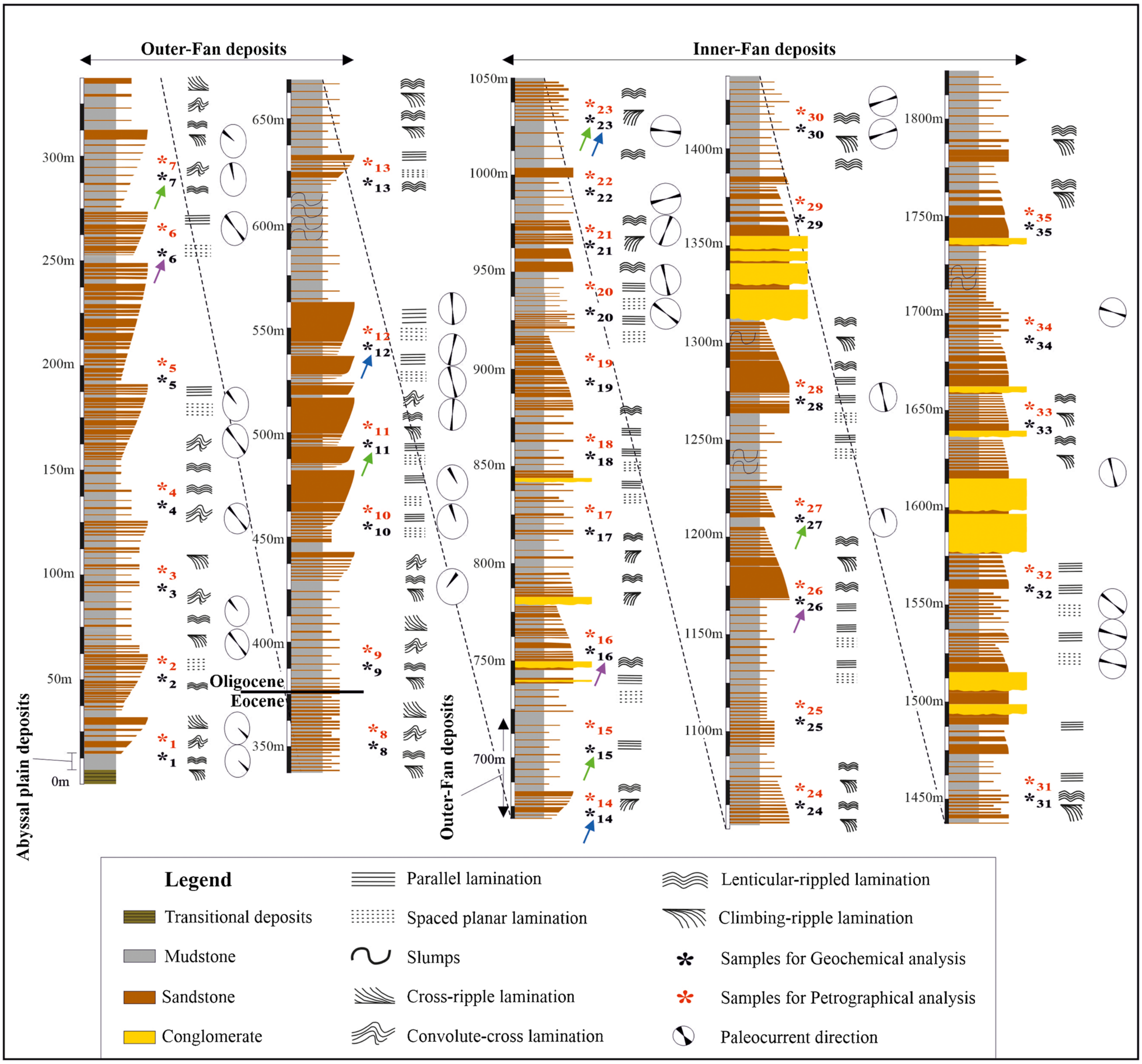

Fig. 4 Representative stratigraphic log of the studied deposits (modified by Botziolis et al. 2021) displaying the relevant analysed samples for geochemical and petrographic study. The outer fan deposits (with a general upward increase in the thickness and abundance of sandstone beds) overlying abyssal plain deposits and in turn overlain by inner fan deposits (with a general upward decrease in the thickness and abundance of sandstone beds). Take note of the consistent paleoflow direction to the northwest. The purple arrow points the samples with the highest V concentration, the green arrow points the samples with the highest Cr concentration and the blue arrow points the samples with the highest Ni concentrations

Analytical methods

Prior to sampling, extensive fieldwork was carried out to identify the study area's sedimentary processes, depositional conditions, and stratigraphic development to ensure that the samples cover the entire sedimentary succession (Figs. 3, 4). For petrographic investigation, 35 samples of very fine- to coarse-grained sandstone were collected (Figs. 3, 4). Thin-sections were cut perpendicularly to the structureless or parallel-laminated sandstone bedding and were petrographically analysed using a B-810 Series Optika Italy polarizing microscope. The detrital assemblages in the samples were identified using the Gazzi-Dickinson point-counting approach by Dickinson (1970).

From classifications derived by just using a petrographic microscope, the origin of quartz, the main constituent of most sandstones, still cannot be ascertained (Götze and Zimmerle 2000). Thus, stricter limitations have been imposed using

Fig. 5 Photographs of outcrops depicting the stratigraphic evolution of the southern PFB. The outer fan deposits are overlain by abyssal plain deposits, which are overlain by inner fan deposits

technically improved cathodoluminescence. Six quartz types can be distinguished, which serve as a guide to provenance. By distinguishing between various feldspar and rock fragment types, cathodoluminescence petrography (CL) may also offer quantitative estimates of their abundance. Moreover, CL enables the estimation of the original grain size and roundness characteristics and enhances the separation of detrital grains from syntaxial overgrowths in well-cemented sandstones. In this work, a Canon Powershot A630 digital camera was used in conjunction with a Reliotron III Cathodoluminescence device linked to a Leitz Wetzlar Orthoplan Microscope to investigate the CL (Liritzis et al. 2019). This CL configuration enables observation of low luminous minerals on exposed thin sections as well as viewing of a reasonably broad area of the sample under cathodoluminescent, plane-polarized, and cross-polarized light (Sippel 1965, 1968; Zinkernagel 1978). In this technique, the thin sections are blasted with electrons using an electron gun that operates at an accelerating voltage of 10 kV and a current of 0.200 mA at an operating vacuum of 100 mTorr, resulting in an electromagnetic phenomenon that may have visible spectrum wavelengths.

Additionally, 35 samples of mudstone were collected (Figs. 3, 4) for geochemical analysis at Bureau Veritas Commodities Canada Ltd. (formerly ACME Analytical Laboratories Ltd., Canada). Inductively coupled plasma optical emission spectrometry (ICP-OES), which has a high degree of accuracy and a low detection limit, was used to analyse major elements, while inductively coupled plasma mass spectrometry (ICP-MS) was used to analyse trace and rare earth elements (REE). To assure appropriateness for comparison with contemporary, well-known tectonic environments, geochemical investigations of sedimentary rocks are recalculated dry (Rollinson 1993). The loss on ignition (LOI) was calculated, and the contents of the principal elements were utilized in several plots after recalculating to an anhydrous (LOI-free) basis and adjusting to 100% for statistical coherence. Major oxide ratios and discriminant functions were calculated to distinguish tectonic setting. Dickinson et al. (1983) ternary diagrams and Verma and Armstrong-Altrin (2013) discriminant-function-based multidimensional diagrams for sediments with high and low silica concentrations, respectively, were employed to establish the tectonic setting of the sediments.

Sandstone petrographic analysis

The samples are very fine- to coarse-grained sandstones, poorly- to very well-sorted, with angular to sub-rounded grains (Figs. 6, 7). According to Garzanti (2016), the majority of samples are feldspatho-quartzo-lithic to feldspatho-litho-quartzose (Fig. 8).

Monocrystalline quartz in the samples range from 21.67 to 37.67% (mean value: 28.22%), whereas lithic fragments range from 2.67 to 12.67% (mean value: 8.77%) (Table 1). Quartz frequently exhibits undulose extinction, whereas polycrystalline quartz, feldspar, biotite, and muscovite are less common (Figs. 6, 7). Tortosa et al. (1991) observed a distinct pattern in sediment composition. They found that sediments originating from granitic and gneissic formations tend to have Qp grains with a limited number of crystals, typically five or fewer. On the other hand, sediments sourced from low-rank metamorphic environments exhibit a prevalence of polycrystalline quartz grains, characterized by more than five fine-very fine crystals. This discrimination based on grain characteristics provides valuable insights into the provenance and geological history of these sediments and for this reason. While the concentration of tectonic quartz (Qt) (including the polycrystalline quartzs with more than 5 splits and undulosed quartz) ranges from 15.33 to 37.67% (mean value: 28.41%), that of polycrystalline quartz without tectonic fabric (Qp) (less than 5 splits) ranges from 2.67 to 6.00% (mean value: 2.91%). Only a few of the quartz grains are well-rounded, with the most being sub-rounded to sub-angular (Figs. 6, 7). All samples contain higher content of plagioclase (ranges between 2.67 and 14.33%, with a mean value: 11.50%), compared to K-feldspar (3.33 to 8.33%, mean value: 5.60%). Many plagioclase crystals exhibit multiple albite twinning (Fig. 6). The content of chlorite and mica (shared by muscovite and biotite), varies from 0.33 to 8.00% (mean value: 4.60%). Mica crystals are mostly elongated (Fig. 6). Rare chlorite and composite grains made of quartz, K-feldspar, plagioclase, and mica are also present. Lithic clasts include fragments of sedimentary rocks such as chert, sandstone, shale, and limestone as well as low-grade metamorphic rocks such as slate and quartz-schist (Fig. 6). Sandstone fragments are mostly sub-angular to sub-rounded and range from 2.34 to 11.00% (mean value: 7.62%) (Fig. 6). Chert fragments (Fig. 6) are mostly sub-angular to sub-rounded, but rounded grains also occur and their abundance ranges from 2.67 to 18.00% (mean value: 9.05%). Slate and schist fragments are mostly sub-angular and vary between 0.33 and 1.67% (mean value: 1.05%) (Fig. 6).

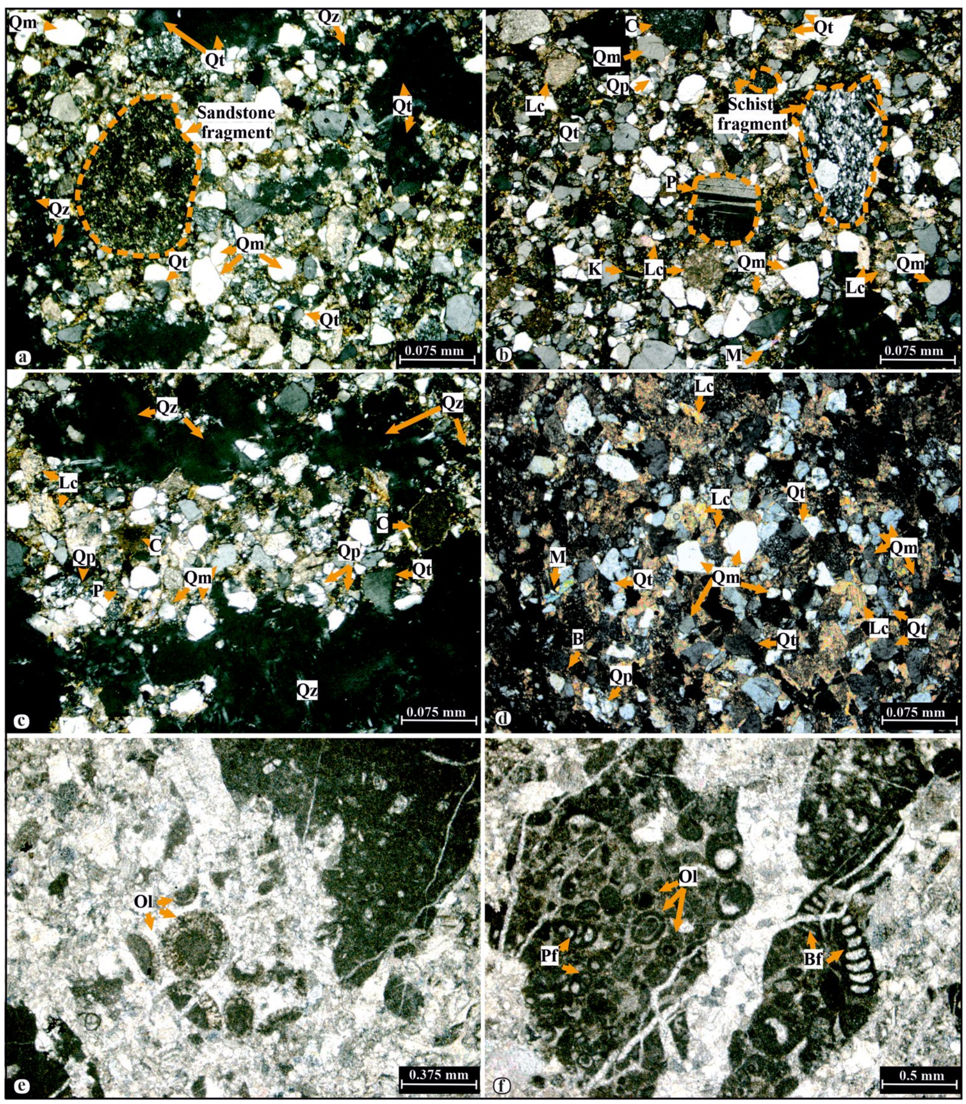

Fig. 6 Representative photomicrographs illustrating the petrographic features of the sandstones from the Upper Eocene-Lower Oligocene PFB deposits. **a** Presence of sandstone fragment, monocrystalline quartz (Qm) and tectonic quartz (Qt) displaying undulose extinction; **b** schist fragment, along with plagioclase (P) showing repeated twinning; **c** chert and polycrystalline quarts (Qp), **d** tectonic quartz (Qt) displaying fracturing; **e** detrital quartz and limestones with oolite fragments; **f** detrital oolite and foraminifera fragments in calcite matrix. All are taken under crossed nicols. Abbreviations: Qp: polycrystalline quartz; Qm: monocrystalline quartz; Qt: tectonic quartz; Qz: quartz in matrix; P: plagioclase; K: K-feldspar; C: chert; B: Biotite; M: muscovite; Bf: benthic foraminifera; Pf: planktonic foraminifera; Ol: oolite and Lc: lithic calcite

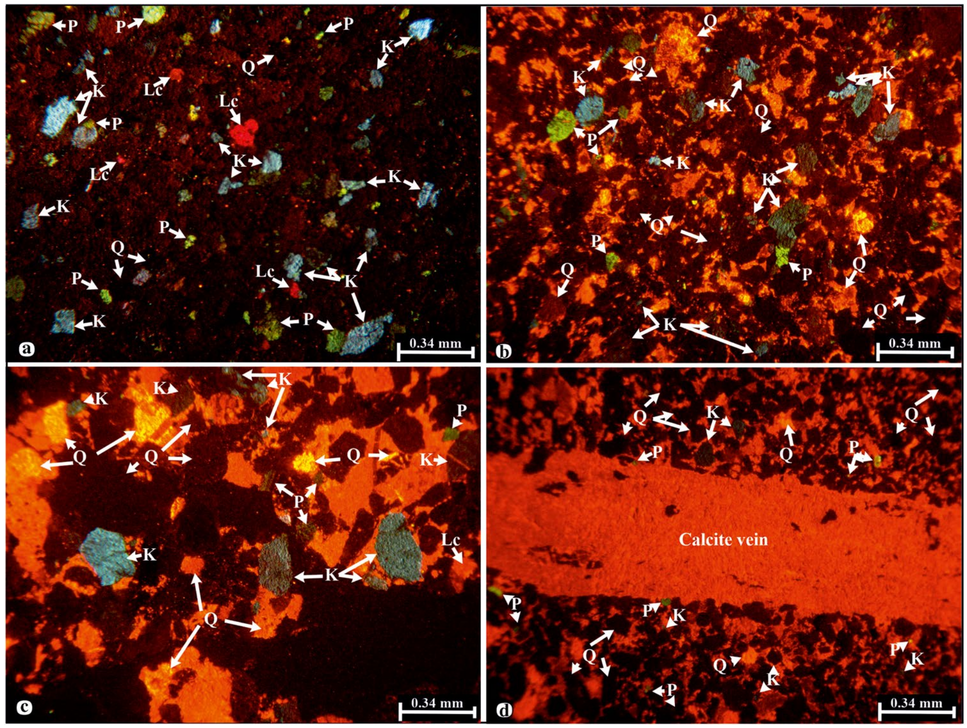

Fig. 7 CL photomicrographs (**a**-**d**) illustrating the petrographic features of the sandstones from the Upper Eocene-Lower Oligocene PFB deposits, under cathodoluminescence. Abbreviations: Q: quartz; P: plagioclase; K: K-feldspar; Lc: lithic calcite

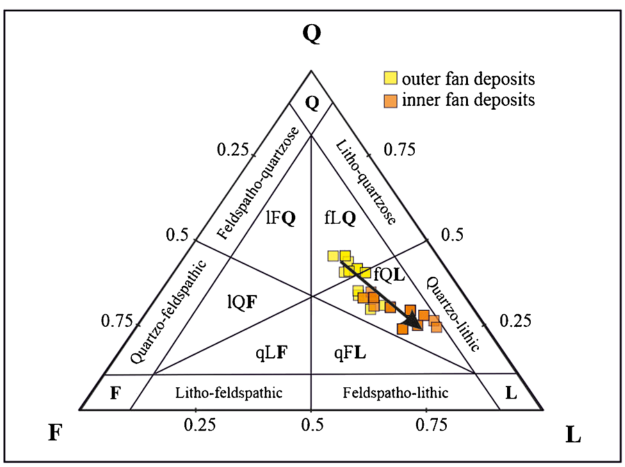

Fig. 8 Ternary diagrams (after Garzanti 2016) showing provenance fields defined by total quartz, feldspar and unstable (nonquartzose) lithic fragments. Abbreviations: Q = quartzose; F = feldspathic; L = lithic; lFQ = litho-feldspatho-quartzose; lQF = litho-quartzo-feldspathic; qLF = quartzo-litho-feldspathic; qFL = quartzo-feldspatho-lithic; fQL = feldspatho-quartzo-lithic; fLQ = feldspatho-litho-quartzose

Cathodoluminescence can be used to investigate the differentiation and origin of sandstone detrital grains more effectively in sedimentary rocks (Götze and Zimmerle 2000). High-temperature crystallization and rapid cooling produce red or bright blue luminescing quartz, which is frequently found in volcanic rocks or rocks that have experienced contact metamorphism (Boggs et al., 2002). Slower cooling and lower crystallization temperatures cause the CL signal in quartz to be less intense, turning the grain from typically bright to dark blue. This kind is common in plutonic rocks because they cool more slowly than volcanic rocks (Boggs et al., 2002). According to Zinkernagel (1978), non-luminous quartz is formed diagenetically or crystallizes below around 300 °C. The authigenic quartz CL colours range from light blue to green to reddish brown (Ramseyer et al. 1988; Neuser et al. 1989). Quartz grains may lose their CL colour and often have a brown colour due to local metamorphism and acquire a blue hue by high-grade metamorphism (Boggs et al., 2002). In the studied samples, quartz crystals with red and brown tones were observed. Optical classification of the quartz crystals revealed that 22% of them were brown quartz and 78% were red quartz (Fig. 7). Additionally, plagioclase crystals emit a greenish yellow colour, feldspar crystals emit a vivid blue colour and carbonate minerals an orange-red colour (Fig. 7).

Mudstone geochemical analysis

Major elements abundances

The major elements abundances document that the studied sediments have slightly lower SiO_2, Al_2O_3, K_2O, TiO_2, P_2O_5 contents (on average 59.56 wt.%, 14.70 wt.%, 2.68 wt.%, 0.77 wt.% and 0.12 wt.%, respectively) relative to the Post-Archaean Australian Shale (PAAS, 62.80 wt.%, 18.90 wt.%,

Table 1 Point-counting data (% percentage) for the PFB system. Three hundred points were counted per thin-section by utilizing the Gazzi-Dickinson method

	Min	Max	Average	
Qm	21.67	37.67	28.22	Sub-grains > 0.063 mm (no splitting)
Qp	0.33	6.00	2.91	Sub-grains < 0.063 mm and < 5 grains splitting
Qt	15.33	37.67	28.41	Undulose extinction or sub-grains < 0.063 mm and > 5 grains splitting
C	2.67	18.00	9.05	
P	2.67	14.33	11.50	Twinned, non-twinned, sericitized, etc.
K	3.33	8.33	5.60	Microcline, orthoclase, perthitic
Ls	2.67	12.67	8.77	Micritic-sparitic limestone, sandstone, schist, slate fragments
Tqm	0.00	1.33	0.29	Quartz eFeldspar, muscovite, biotite
Mp	0.00	2.33	0.62	Quartz-bearing phyllite
M	0.33	8.00	4.60	Muscovite, biotite, chlorite
Q	29.66	51.33	40.18	
F	2.67	14.33	11.50	
L	23.00	49.00	38.09	
Qm	21.67	37.67	28.22	
Lt	36.00	66.33	50.05	
Qmp	23.00	43.33	31.13	
R	31.00	64.67	47.14	

3.70 wt.%, 1.00 wt.% and 0.16 wt.%, respectively, McLennan et al. 1993) (Table 2). On the other hand, the average abundances of MgO, CaO and Na_2O (4.08 wt.%, 9.18 wt.% and 1.50 wt.%, respectively) are enriched relative to PAAS (2.20 wt.%, 1.30 wt.% and 1.20 wt.%, respectively, McLennan et al. 1993) (Table 2). The mean contents of Fe_2O_3 and MnO are 7.01 wt.% and 0.09 wt.%, respectively, similar to PAAS (7.10 wt.% and 0.11 wt.%, respectively, McLennan et al. 1993) (Table 2). LOI values range from 7.6 to 17.9 wt.% (Table 2).

The relationship between minerals and the distribution of major elements can be documented by the Pearson correlation coefficient variations of selected major elements (SiO_2, TiO_2, and K_2O) versus Al_2O_3 (Bauluz et al. 2000). Al_2O_3 was selected because Al is immobile throughout weathering and diagenesis (Bauluz et al. 2000). In the PFB samples, SiO_2 displays a weak negative linear correlation with Al_2O_3 (r = −0.17) (Fig. 9). In contrast, K_2O, TiO_2, and Al_2O_3 demonstrate a strong positive linear correlation (r = 0.95 and 0.95, respectively) (Fig. 9). All samples display K_2O/Al_2O_3 ratios below 0.21.

Trace element abundances

The trace element values were normalized against the PAAS to evaluate the degree of enrichment or depletion and to determine the source of the sediments (Fig. 10). Certain Large Ion Lithosphere Elements (LILEs) like Rb, Cs, Ba, and Sr, some High Field Strength Elements (HFSEs) like Nb, Zr, Th, and U, and other trace elements like Ga and Ta have lower concentrations when compared to PAAS (Table 2). Other trace elements, such as Cr, Ni, Cu, Pb and Zn are enriched compared to PAAS (Table 2). Elements like Sr (LILE), Sc, Hf (HFSEs), and a few other trace elements (Co, V, and Y) are comparable to those of PAAS (Table 2).

Pearson correlation coefficient variations of some trace elements (Ba, Rb, Th, V and Ni) against Al_2O_3 and Zr against SiO_2 document the relationship between the minerals and the trace elements distribution (McLennan et al. 1993; Chen et al. 2014; Ali et al. 2014). In the PFB, Ba displays moderate positive linear correlation with Al_2O_3 ($r = 0.76$) (Fig. 9). Rb, Th and V demonstrate a strong positive correlation with Al_2O_3 ($r = 0.96$, 0.93 and 0.99, respectively) (Fig. 9). Ni exhibits a weak negative linear correlation with Al_2O_3 ($r = -0.09$) while, Zr displays a moderate positive linear correlation with SiO_2 ($r = 0.65$) (Fig. 9).

Rare earth elements (REE)

The samples average total REE content is 120.82 ppm, with a range of 90.86 to 168.42 ppm (Table 2). Light REE (LREE, La, Ce, Pr, Nd, Sm, and Eu) to heavy REE (HREE, Gd, Tb, Dy, Ho, Er, Tm, Yb, Lu, and Y) ratio is high (7.34 on average) (Table 2). The average $(La/Yb)_N$ and $(La/Sm)_N$ ratios of 7.41 and 3.46, respectively, where subscript N refers to chondrite-normalized values, support the moderate enrichment in light REE (LREE) patterns. The samples also exhibited relatively flat heavy REE (HREE) patterns (Fig. 11), confirmed by the $(Gd/Yb)_N = 1.50$ ratio. N-MORB normalised patterns for the PFB samples reveal high contents of Rb, Th and Ba, along with Nb, Sr and Ti depletion (Fig. 12). The samples display a negative Eu anomaly [$(Eu/Eu^* = (Eu)_N/((Sm)_N \times (Gd)_N)1/2)$] ($Eu/Eu^* = 0.71$, average), and any Ce anomaly [$(Ce/Ce^* = (Ce)_N/((Pr)_N$^2 / $(Nd)_N))$] ($Ce/Ce^* = 0.88$, average) is lacking (Table 2).

Table 2 Major elements (in wt.%) after LOI correction, trace elements, rare earth elements (REE) (in ppm) and elemental ratios for the PFB system

	Min	Max	Average	PAAS (*)		Min	Max	Average	PAAS (*)		Min	Max	Average	PAAS (*)
SiO_2	52.97	68.56	59.56	62.8	**Cr**	334.08	1056.91	469.63	110.00	**La**	18.60	35.50	24.89	38.20
Al_2O_3	10.01	17.73	14.70	18.9	**Ba**	218.00	361.00	281.06	650.00	**Ce**	36.20	62.40	48.74	79.60
Fe_2O_3	3.96	8.72	7.01	7.10	**Co**	9.20	32.90	20.95	20.00	**Pr**	4.29	8.47	5.66	8.83
MgO	1.69	6.27	4.08	2.20	**Ni**	77.00	312.00	172.91	55.00	**Nd**	16.40	31.50	21.74	33.90
CaO	0.77	17.52	9.18	1.30	**Cs**	2.50	15.90	4.97	15.00	**Sm**	3.22	6.35	4.33	5.55
Na_2O	0.85	1.87	1.50	1.20	**Ga**	7.20	18.20	13.74	17.50	**Eu**	0.72	1.57	0.97	1.08
K_2O	1.79	3.57	2.68	3.70	**Hf**	2.80	4.80	3.74	5.00	**Gd**	3.09	6.35	4.03	4.66
TiO_2	0.54	0.93	0.77	1.00	**Nb**	6.40	11.80	9.41	19.00	**Tb**	0.49	1.04	0.64	0.774
P_2O_5	0.09	0.19	0.12	0.16	**Rb**	58.10	131.80	97.93	160.00	**Dy**	3.00	6.11	3.80	4.68
MnO	0.05	0.15	0.09	0.11	**Sr**	81.30	228.30	173.72	200.00	**Ho**	0.59	1.26	0.79	0.991
LOI	7.60	17.90	12.40		**Ta**	0.40	0.90	0.67	1.28	**Er**	1.83	3.62	2.34	2.85
Al_2O_3/TiO_2	17.51	21.35	19.02	18.90	**Th**	5.80	10.50	8.10	14.60	**Tm**	0.27	0.52	0.34	0.405
K_2O/Al_2O_3	0.17	0.21	0.18	0.20	**U**	1.60	2.70	2.03	3.10	**Yb**	1.69	3.26	2.22	2.82
CIA	66.29	77.36	71.98	75.30	**V**	69.00	160.00	124.06	150.00	**Lu**	0.25	0.47	0.34	0.433
ICV	1.02	2.63	1.76	0.88	**Zr**	103.10	177.20	140.50	210.00	**LREE**	79.49	145.79	120.82	167.16
					Y	15.40	33.90	21.05	27.00	**HREE**	11.37	22.63	14.50	17.61
					Cu	23.20	64.30	39.43	28.00	**LREE/HREE**	6.44	7.86	7.34	9.49
					Pb	8.70	158.10	25.57	20.00	**$(La/Yb)_N$**	6.80	7.95	7.41	8.95
					Zn	60.00	117.00	89.06	67.00	**$(Gd/Yb)_N$**	1.39	1.69	1.50	1.37
					Sc	9.00	20.00	15.83	16.00	**$(Sm/Yb)_N$**	1.94	2.42	2.14	2.16
					Cr/V	2.41	9.52	3.96	0.73	**$(Sm/Gd)_N$**	165.06	668.93	295.91	429.05
					Y/Ni	0.05	0.23	0.13	0.49	**$(La/Sm)_N$**	3.19	3.78	3.46	4.14
					Th/Sc	0.44	0.64	0.51	0.91	**Eu/Eu***	0.65	0.78	0.71	0.65
					Zr/Sc	5.42	16.37	9.14	13.13	**Ce/Ce***	0.72	0.95	0.88	0.99
					La/Th	2.82	3.38	3.09	2.61					
					Cr/Ni	2.15	5.29	2.79	2.00					
					Co/Th	1.37	4.11	2.65	1.36					

*Post-Archean average Australian Shale (values after Nance and Taylor, 1976; McLennan, 1981, McLennan 1989; Taylor and McLennan 1995; Barth et al., 2000).

CIA = molar $[Al_2O_3 / (Al_2O_3 + CaO + Na_2O + K_2O)] * 100$

ICV = $(Fe_2O_3 + K_2O + Na_2O + CaO + MgO + MnO + TiO_2) / Al_2O_3$

N refers to chondrite normalized value.

Eu/Eu* = $(Eu)_N / ((Sm)_N * (Gd)_N) * 1/2)$

Ce/Ce* = $(Ce)_N / ((La)_N * (Pr)_N)$ ^ 1/2

	SiO2	Al2O3	K2O	TiO2	Ba	Rb	Sr	Th	U	Zr	Y
SiO2	1.00	-0.17	-0.21	-0.04	-0.01	-0.19	-0.51	0.02	0.21	0.65	0.32
Al2O3		1.00	0.95	0.95	0.76	0.96	-0.49	0.93	0.55	0.14	0.75
K2O			1.00	0.85	0.78	0.99	-0.42	0.88	0.48	0.05	0.65
TiO2				1.00	0.70	0.87	-0.64	0.91	0.68	0.35	0.82
Ba					1.00	0.74	-0.48	0.69	0.41	0.06	0.63
Rb						1.00	-0.42	0.90	0.46	0.10	0.69
Sr							1.00	-0.47	-0.60	-0.46	-0.70
Th								1.00	0.62	0.36	0.82
U									1.00	0.60	0.69
Zr										1.00	0.53
V											1.00

	SiO2	Al2O3	K2O	TiO2	Hf	Cr	V	Sc	Co	Ni	Cu
SiO2	1.00	-0.17	-0.21	-0.04	0.61	-0.25	-0.22	-0.24	-0.61	-0.56	-0.13
Al2O3		1.00	0.95	0.95	0.28	-0.46	0.99	0.97	0.20	-0.09	0.83
K2O			1.00	0.85	0.18	-0.42	0.93	0.91	0.23	-0.05	0.83
TiO2				1.00	0.47	-0.45	0.93	0.91	0.08	-0.14	0.72
Hf					1.00	-0.50	0.25	0.21	-0.43	-0.64	0.17
Cr						1.00	-0.36	-0.31	0.24	0.78	-0.47
V							1.00	0.97	0.24	-0.01	0.83
Sc								1.00	0.27	0.05	0.80
Co									1.00	0.59	0.19
Ni										1.00	-0.09
Cu											1.00

-1	negative correlation
-0.7	
-0.5	
-0.3	
0	
0.3	positive correlation
0.5	
0.7	
1	

Fig. 9 Selected major and trace element Pearson's coefficient correlation variations presented in table for the samples from the southwestern PFB. Major element data are calculated on an anhydrous normalized basis

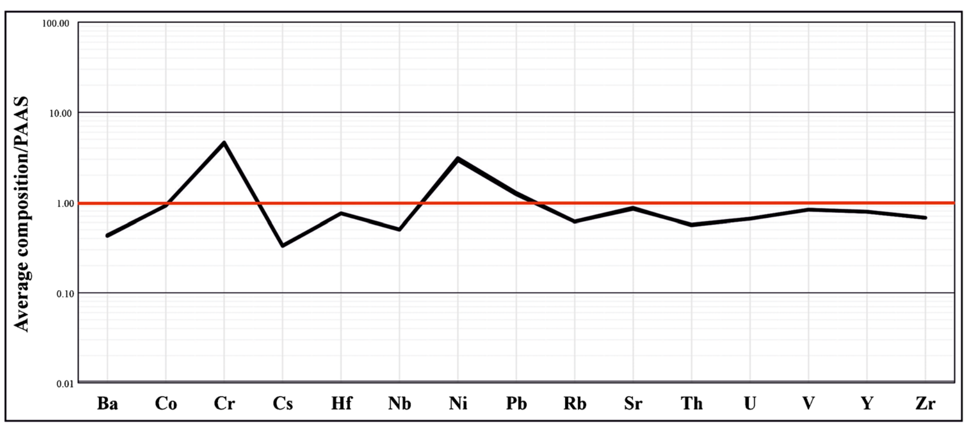

Fig. 10 Post-Archaean Australian Shale (PAAS)-normalized (McLennan et al. 1993) multi-element diagram for the trace element concentrations of PFB

Discussion

The type of source rock, the rate of sediment supply, the degree of sorting during transit and deposition, and the degree of weathering all impact the petrographical and chemical composition of clastic deposits (McLennan 1989; Cox et al. 1995; Roddaz et al. 2006). Therefore, before making inferences about the provenance of sediments and the regional tectonic setting, each of these characteristics must be evaluated.

Source area weathering

SiO_2 and Al_2O_3 in the PFB samples exhibit a moderate negative correlation, indicating that quartz and aluminous clays during deposition hydrodynamically separate (Purevjav and Roser 2013). The strong positive correlation between K_2O and Al_2O_3 and the low K_2O/Al_2O_3 ratios (less than 0.3) suggests that K is found in phyllosilicates or clay minerals (Cox et al. 1995). Ba was absorbed into phyllosilicate minerals in addition to K-feldspar, as shown by the exceptionally strong

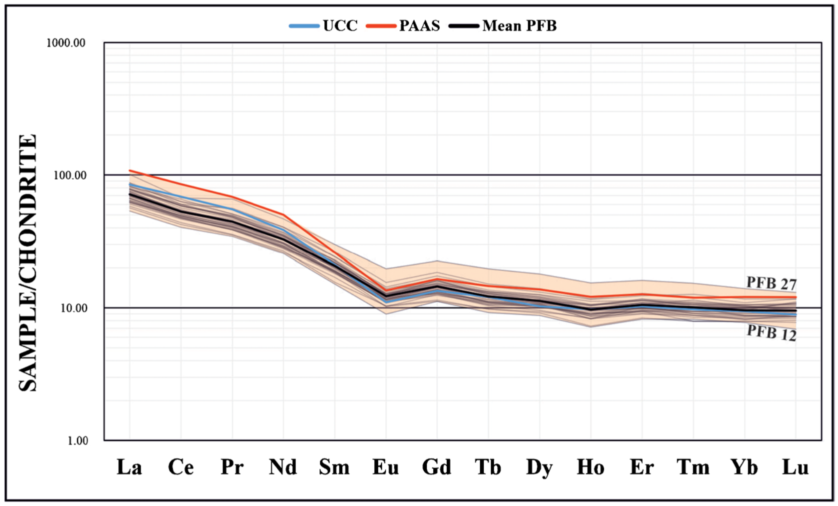

Fig. 11 Chondrite-normalized rare earth element patterns. Chondrite normalization values are from Taylor and McLennan (1985). REE patterns of Post-Archean Australian Shale (PAAS) and Upper Continental Crust (UCC) are included for comparison

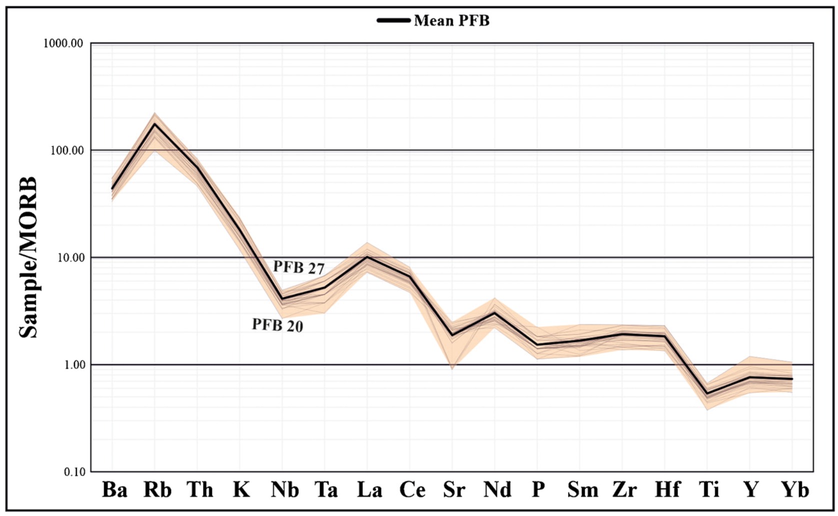

Fig. 12 Mid-ocean ridge basalt (MORB)-normalised spider diagrams for the PFB samples. Normalising values after Pearce (1982)

positive correlation of Ba with Al_2O_3 and K_2O (Fig. 9) (McLennan et al. 1993). According to Fig. 9, the moderate positive correlation between Rb and Al_2O_3 indicates that the Rb is mostly present in phyllosilicate minerals (McLennan et al. 1993). Th is concentrated in clay minerals rather than accessory minerals, according to the strong positive correlation of Th with Al_2O_3 (Fig. 9) (Armstrong-Altrin et al. 2015; Etemad-Saeed et al. 2015; Amendola et al. 2016). The weak positive correlation of Zr with SiO_2 (Fig. 9) suggests that Zr is present in the rock silicate component. The strong positive correlation between Al_2O_3 and V (Fig. 9) suggests that the V content increases with increasing Al_2O_3 content. This correlation can be attributed to the association of V with Al-rich phases, such as clay minerals. Because Al_2O_3 and Ni have a weak negative correlation, the concentration of Ni in heavy minerals or relict mafic minerals is most likely what controls how the element is distributed (Fig. 9).

The PFB mudstones of the foredeep depozone compared to the PAAS mudstones are depleted in SiO_2, Hf and Zr and enriched in Cr and Ni (Table 2, Fig. 10). Quartz dilution caused by the loss of unstable phases and relative zircon concentrations is the most likely cause (Roddaz et al. 2006). In contrast to PAAS, Na_2O, CaO, MgO, and Sr are more enriched than K_2O, Rb, and Ba. Plagioclase, a rapidly weathering mineral with more Na, Ca, and Sr than minerals containing Rb, Ba, and K, is responsible for this trend (White and Brantley 1995). Furthermore, strong positive correlations have been observed between Rb and Ba with K_2O (Fig. 9), indicating that the distribution of these elements might be influenced by the presence of alkali-feldspar (Armstrong-Altrin et al. 2014). Another explanation is the immobilization of smaller cations such as Na, Ca, and Sr rather than bigger cations such as K, Cs, Rb, and Ba because of adsorption and absorption on clay mineral surfaces (Nesbitt et al. 1980; Wronkiewicz and Condie 1990; Bauluz et al. 2000; Roddaz et al. 2006).

The Chemical Index of Alteration (CIA index) is a widely used method for estimating the degree of weathering at the source location (Nesbitt and Young 1982; Fedo et al. 1995, 1996; Bauluz et al. 2000; Lee 2002; Hofmann et al. 2003). The formula CIA = [Al_2O_3 / (Al_2O_3 + CaO*, Na_2O, and K_2O)] * 100 is used to calculate the amount of feldspar weathering in comparison to unaltered protoliths (molar proportions). CaO* stands for the concentration of the silicate component. Because we do not have CO_2 contents for the samples, we are unable to account for Ca in carbonates. As a result, CaO values are accepted if the mole fraction of CaO is equal to or less than Na_2O and the moles of CaO are equal to Na2O if CaO values are greater than Na_2O (McLennan et al. 1993; Bock et al. 1998; Jian et al., 2013). According to Garzanti and Resentini (2015), no matter what correction method is used, CIA control remains resilient. In Fig. 13a, the CIA values are displayed. Unmodified upper crustal rocks and unaltered plagioclase and K-feldspar have CIA values that are nearly equal to 50. Higher CIA values imply increase in weathering.

The compositional maturity of mudstones is assessed using the Index of Compositional Variability (ICV) (Cox et al. 1995). It can be utilized to determine if the rocks in the provenance experienced sediment recycling (Cullers and Podkovyrov 2000). The ICV formula uses the following chemical ratios: ICV=(Fe_2O_3+K_2O+Na_2O+CaO+Mg O+MnO+TiO_2)/$A1_2O_3$. Compositionally immature mudstones are typically deposited in tectonically active settings and have ICV values higher than one (1) (Cullers and Podkovyrov 2000) due to a large percentage of non-clay silicate minerals (Van de Kamp and Leake 1985). By contrast, compositionally mature mudstones generated in a passive margin (Weaver, 1989) have ICV values smaller than one (1) (Cullers and Podkovyrov 2000). Figure 13a depicts the ICV values. The samples ICV and CIA values (mean 1.73 and 72.18, respectively) indicate that they originated from immature source rocks with low to moderate source weathering (Fig. 13a). The Al_2O_3 - CaO* + Na_2O - K_2O (A-CN-K)

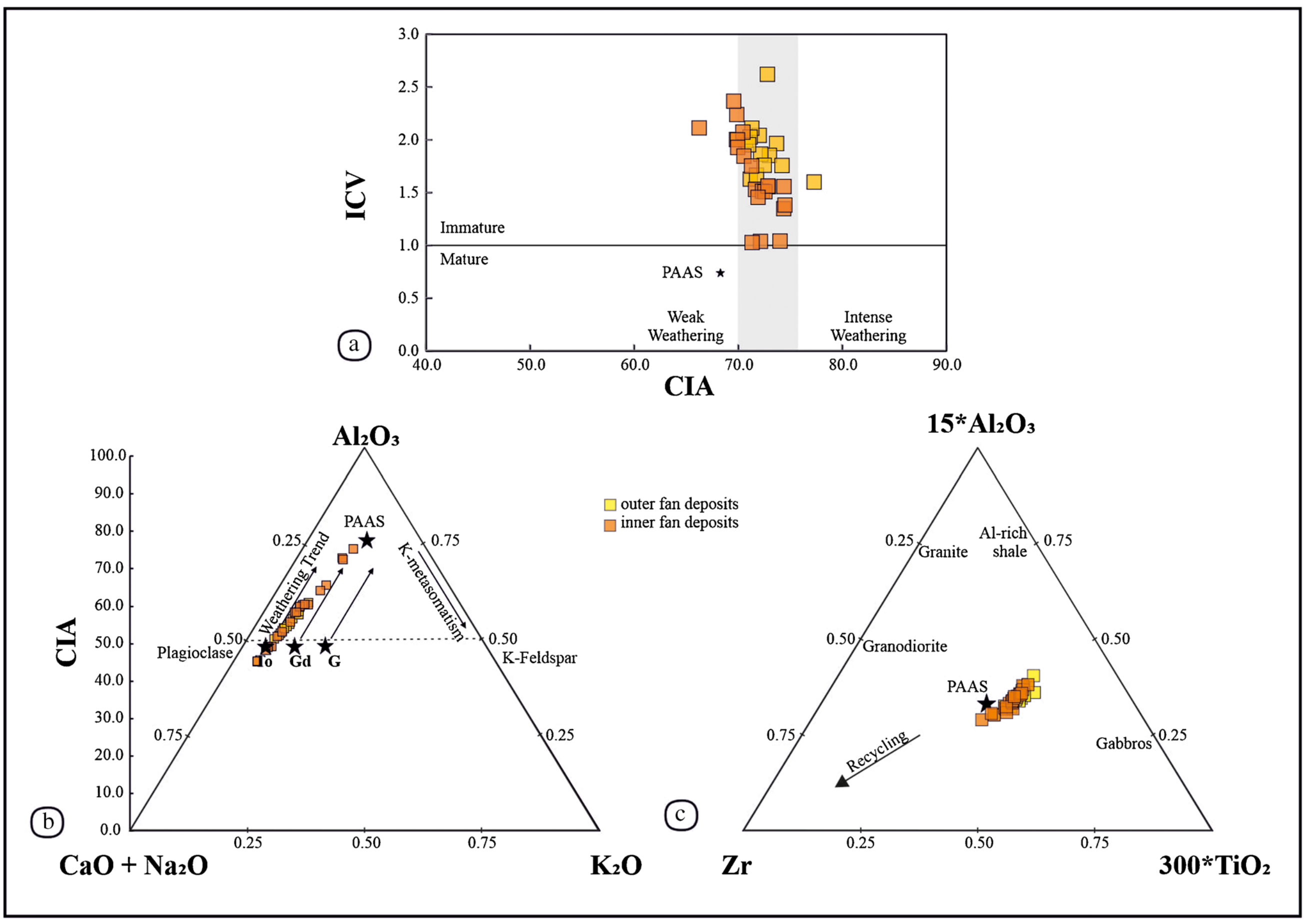

Fig. 13 **a** Chemical Index of Alteration (CIA) against Index of Compositional Variability (ICV) diagram for the sedimentary rocks in the central PFB (after Nesbitt and Young 1984; Cox et al. 1995). PAAS composition taken from Taylor and McLennan (1985). **b** CIA and ternary A-CN-K diagram (after Nesbitt and Young 1982; McLennan et al. 1993) for the sedimentary rocks of PFB. PAAS (Taylor and McLennan 1995) is plotted for comparison. Average tonalite (T), granodiorite (Gd) and granite (G) compositions shown are taken from Condie (1993). Predicted weathering trends (arrows) of T, Gd and G are also shown. **c** $15Al_2O_3$-Zr-300*TiO_2 ternary diagram (Garcia et al. 1991)

ternary diagram can be used to determine the level of weathering (Nesbitt and Young 1984). The samples in this diagram are near the Pl-Ks tie line and progress towards the Al_2O_3 apex, following and parallel to the projected tonalite-granodiorite weathering pattern (Fig. 13b). These characteristics provide a weathering trend that deviates from the fundamental composition of tonalite (Fedo et al. 1995). The degree of weathering across the various samples is mostly similar, resulting in a compact group throughout the tonalite weathering trend (Fig. 13b), indicating weathering conditions that remained constant (Nesbitt et al. 1997) for the Late Eocene to Early Oligocene PFB mudstones.

Sedimentary processes, sorting and recycling

Sedimentary processes may significantly alter mineral abundances, which in turn affects the concentrations of certain elements. Our sediments include a variety of grain sizes, from mudstone to very fine sandstone. Contrary to coarser-grained sediments, fine-grained sediments have a chemical composition that is identical to that of their source (Cullers 1994, 2000). The SiO_2/Al_2O_3 ratios can be used to measure the textural maturity (McLennan et al. 1993), ranging from 3.19 to 6.85 and are typically greater than those of PAAS (3.3). Plagioclase may be incorporated into mudstones because of sorting, which would reduce the Eu anomaly (McLennan et al. 1993). This is especially accurate for mudstones created in tectonically active regions (McLennan et al. 1990), where mudstones lack a constant Eu enrichment because of the low percentage of plagioclase in sediments (Nathan 1976; Bhatia 1985; McLennan et al. 1993). Mudstones from the foredeep depozone in the PFB had similar Eu anomalies to those in the PAAS, demonstrating the absence of plagioclase concentration because of sediment physical sorting. In contrast to mature sedimentary rocks, immature source rocks with limited degree of sorting and recycling have a narrower range of TiO_2/Zr variation (Garcia et al. 1991). The samples plot close to the PAAS and show a narrow range of TiO_2/Zr variation, indicating an immature source with low source sorting and sediment recycling (Fig. 13c).

Provenance

The results of this study indicate multiple sources that contributed to the sedimentation of the PFB. Detritus such as monocrystalline and polycrystalline quartz (Qp < 5 splits), plagioclase, K-feldspar, composite quartz-feldspar, and quartz-mica grains provide evidence that the PFB originated from a magmatic source. These results are supported by cathodoluminescence petrography of quartz grains, which shows that detrital monocrystalline quartz is of volcanic origin (red quartz crystal CL color) and, less frequently, of metamorphic origin (brown quartz crystal CL color) (Götze and Zimmerle 2000). Chlorite can be created by the transformation of mafic minerals and volcanic glass. Nevertheless, the presence of detrital minerals of the chlorite group which are well known in low temperature and prograde metamorphic rocks (Deer et al. 2013), provide evidence of a low-grade metamorphic source-rock, which is further confirmed by the occurrence of polycrystalline quartz with more than five splits, as well as slate and schist. Sedimentary sources are another significant contributor that provided debris to the PFB. This source is also made of shale, sandstone, limestone, and chert, according to the thin sections and conglomerates of the study area.

Chemical features reflect the composition of the sources involved in the sedimentation. The homogeneous mixing of the central PFB sediments (Fig. 13c) is attributed to the efficient mixing of the source rock fragments during transit and deposition (McLennan 1989; Vital and Stattegger 2000). The A-CN-K plot pattern indicates that it originated from less felsic parent rocks such as granodiorite (Fig. 13b). TiO_2 vs. $Al2O_3$ graph and moderate to high Al_2O_3/TiO_2 ratios (mean value: 19.02) indicate that the detritus came from felsic rocks similar to that suggested in the A-CN-K plot (Fig. 14a). The REE, Th, and HFSE can be used to evaluate the composition of the rocks in the source areas (Taylor and McLennan 1985; McLennan et al. 1990). These elements become insoluble and immobile during weathering, metamorphism, and they have a low sensitivity to post-crystallization alteration (White et al. 2002; Grosch et al. 2007; Koralay 2010). Furthermore, they are more abundant in felsic rocks than in mafic rocks (Etemad-Saeed et al. 2011) and Th is widely used as a proxy for terrigenous sediment input in marine environments (McManus et al. 2004).

According to McLennan et al. (1993) and the references within, the Eu anomaly is widely assumed to have been acquired from the sediment sources. Large abnormalities are usually attributed to a felsic origin, whereas small Eu anomalies are frequently attributed to mafic debris (Taylor and McLennan 1985; Hassan et al. 1999; Cullers 2000). The PFB samples exhibit Eu anomalies (Eu/Eu* = 0.65–0.78) that are comparable to higher than the average value of PAAS (Eu/Eu* = 0.65), indicating that these sediments were eroded from a mixed source of felsic and mafic origin (Taylor and McLennan 1985). The chondrite-normalized rare earth element (REE) abundances of PFB (Figure 11) are similar to those of UCC and PAAS (enrichment in light rare earth elements (LREE), flat heavy rare earth elements (HREE), and negative Eu anomalies). This similarity suggests that PFB has a differentiated source resembling granite. This conclusion is further supported by the high LREE/HREE ratio (average 7.34), which is a characteristic feature of felsic source rocks (Cullers 1994; Taylor and McLennan 1985; Wronkiewicz and Condie 1990). Elemental ratios

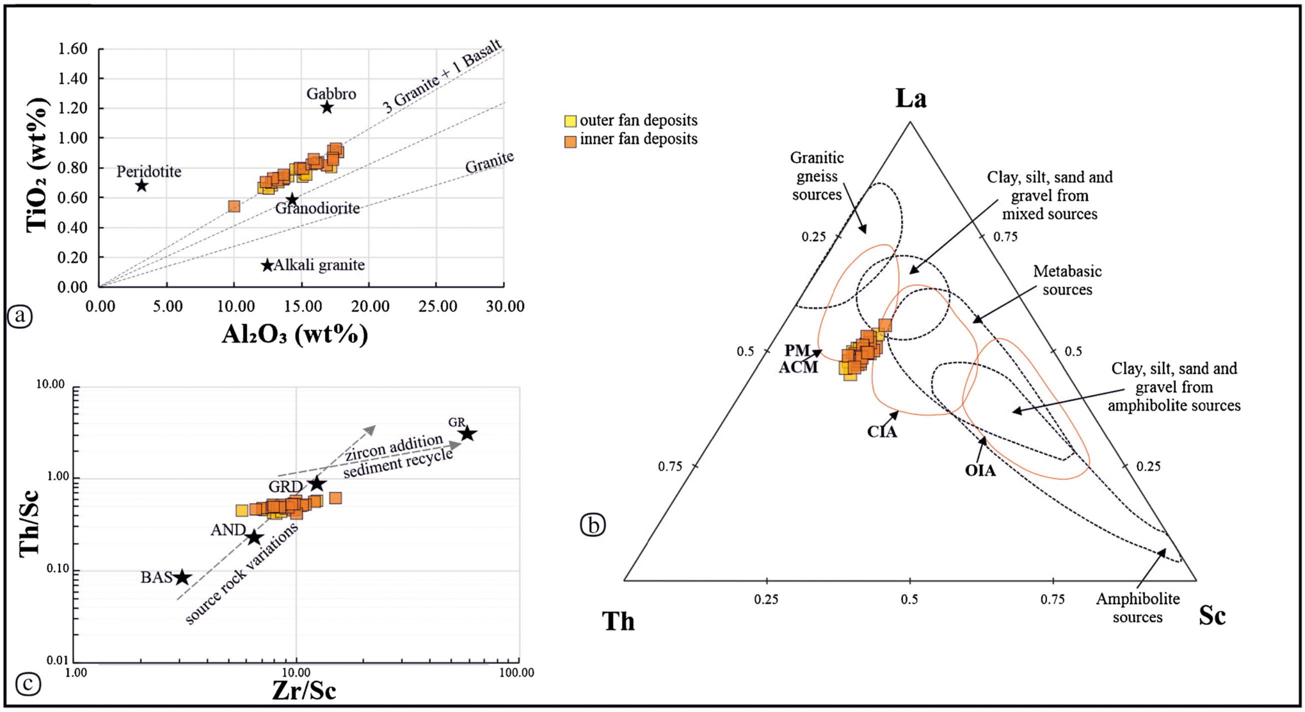

Fig. 14 **a** TiO_2 against Al_2O_3 diagram for the PFB samples. The "granite", "granodiorite" and the "3 granite + 1 basalt" lines are from Schieber (1992), **b** plot of the studied samples on the La-Th-Sc ternary diagram proposed by Cullers (1994). Abbreviations: PM: Passive margin; ACM: Active continental margin; CIA; Continental Island arc; OIA: Oceanic island arc, **c** Th/Sc against Zr/Sc diagram (McLennan et al. 1993) that evaluates the source rock composition of the studied sediments. Abbreviations: BAS, AND, GRD and GR refer to average gabbro, andesite, granodiorite and granite, respectively (Le Maitre 1976)

such as Th/Sc and La/Sc (Table 2) and the presence of the Eu anomaly are easily influenced by the average composition of the source rock (Taylor and McLennan 1985). The significant variations in element ratios among different regions indicate that local source rocks have an influence on sediment composition. The La/Sc ratios (1.33–2.07) and Th/Sc ratios (0.44–0.64) observed in the PFB sediments are not typical of recycled sediments, but instead suggest a higher proportion of felsic components in the source. They are also enriched in Th/U ratios and in HFSE compared to PAAS (Table 2). Therefore, it is probable that the samples are more likely derived from a felsic to upper continental source rather than a predominantly mafic source with little recycling (Taylor and McLennan 1985; Hassan et al. 1999; Bauluz et al. 2000).

The felsic to intermediate source rock composition is further suggested by (1) the La-Th-Sc ternary diagram proposed by Cullers (1994), in which the samples plot at the clay, silt, sand, and gravel from mixed sources field area, between the granitic gneiss to metabasic field (Fig. 14b); (2) LREE enrichment documented by the high $(La/Yb)_N$ ratios; (3) flat HREE segments documented by the $(Gd/Yb)_N$ ratios (Figs. 11) and 4) the negative Eu anomalies. The trace elements Th, Zr, and Sc are used in Fig. 14c because they are typically immobile. This figure is beneficial because passive continental margin sediments exhibit increased Zr/Sc ratios due to zircon enrichment via sediment recycling (McLennan et al. 1993). Active-margin samples, on the other hand, show a trend between mafic and continental origins. Fig. 14 demonstrates that the PFB samples follow this pattern, showing low sediment recycling, despite the presence of slight zircon addition in sandstones (Harper, 1980; Miller and Saleeby, 1995). Furthermore, in the plot of Th/Sc vs Zr/Sc (Fig. 14c), the samples show Th/Sc values that indicate origin from less felsic igneous sources, which is corroborated by the higher Cr and Ni values. Because of their low mobility during sedimentary processes, elements like V, Co, Cr, and Ni are regarded as being useful for determining the origin of sediments (Floyd and Leveridge 1987; McLennan et al. 1993; Rollinson 1993; Cullers 2000). Moreover, the higher Cr and Ni concentrations in the PFB samples (enriched relative to PAAS values) point to a mafic source input. Further evidence for this source type comes from the Cr/V and Y/Ni ratios, as well as the Y/Ni versus Cr/V and Ni against Cr diagrams (Fig. 15a, b).

Tectonic setting

The QFL ternary diagram is used to define the tectonic setting (Garzanti 2019). PBF samples are concentrated in the recycled orogenic field (Fig. 16). Whole-bulk geochemistry, which has been employed by several authors, is used to document the tectonic setting using contemporary visuals (e.g., Verma and Armstrong-Altrin 2013; Zaid and Gahtani 2015; Tawfik et al. 2017; Maravelis et al. 2021). Therefore, in this study, the discriminant-function-based major-element diagram by Verma and Armstrong-Altrin (2013) is utilized to assess the tectonic setting for sedimentary rocks with high (SiO_2 = 63–95%) and low (SiO_2 = 35–63%) silica content. The samples plot in the collision field in both figures (Fig. 17a, b). The La-Th-Sc ternary diagram Cullers (1994) yields the same results, since all samples plot in the active continental margin field (Fig. 14b).

However, stratigraphic and geochemical information should also be taken into account while analysing the tectonic framework (Ryan and Williams 2007; Maravelis et al. 2017). The region under investigation has sustained significant sediment deposition since the Triassic epoch, according to earlier stratigraphic data (Karakitsios 1995; Avramidis and Zelilidis 2001; Sotiropoulos et al. 2003; Papanikolaou 2009). Triassic evaporites that evolved upward into carbonates prevailed, followed by Upper Eocene siliciclastic sedimentation. The PFB system, which progresses from west to east from abyssal plain deposits to outer- and finally into inner-fan deposits, unconformably overlies the Eocene carbonates. The change from carbonate to siliciclastic sedimentation is related to the onset of the formation of Pindos orogen, the transition from a passive to an active continental margin, and the formation of the PFB (Fleury 1980; Degnan and Robertson 1998; Xypolias and Doutsos 2000). The succession's stratigraphic evolution shows a comparable transition from muddy abyssal-plain deposits to sandy outer and sandy/conglomeratic inner fan deposits, illustrating system progradation and the temporal shallowing of the central PFB. In conclusion, the stratigraphic and geochemical data presented here are consistent with an end-Mesozoic and Cenozoic Alpine collision that led to development of the Pindos Orogeny and associated thrusting (Jones and Robertson 1991; Robertson et al. 1991).

Implications for the evolution of the Pindos Orogen — composition trends

During the Late Palaeozoic to Cenozoic, the Apulia microcontinent separated from Gondwana, leading to the formation of a NE-striking rift system and the opening of the Neo-Tethyan Ocean (Robertson et al. 1991; Ricou 1994; Frizon de Lamotte et al., 2011). This process resulted in the development of platforms and basins, as evidenced by sedimentary records. The domains that emerged during Early

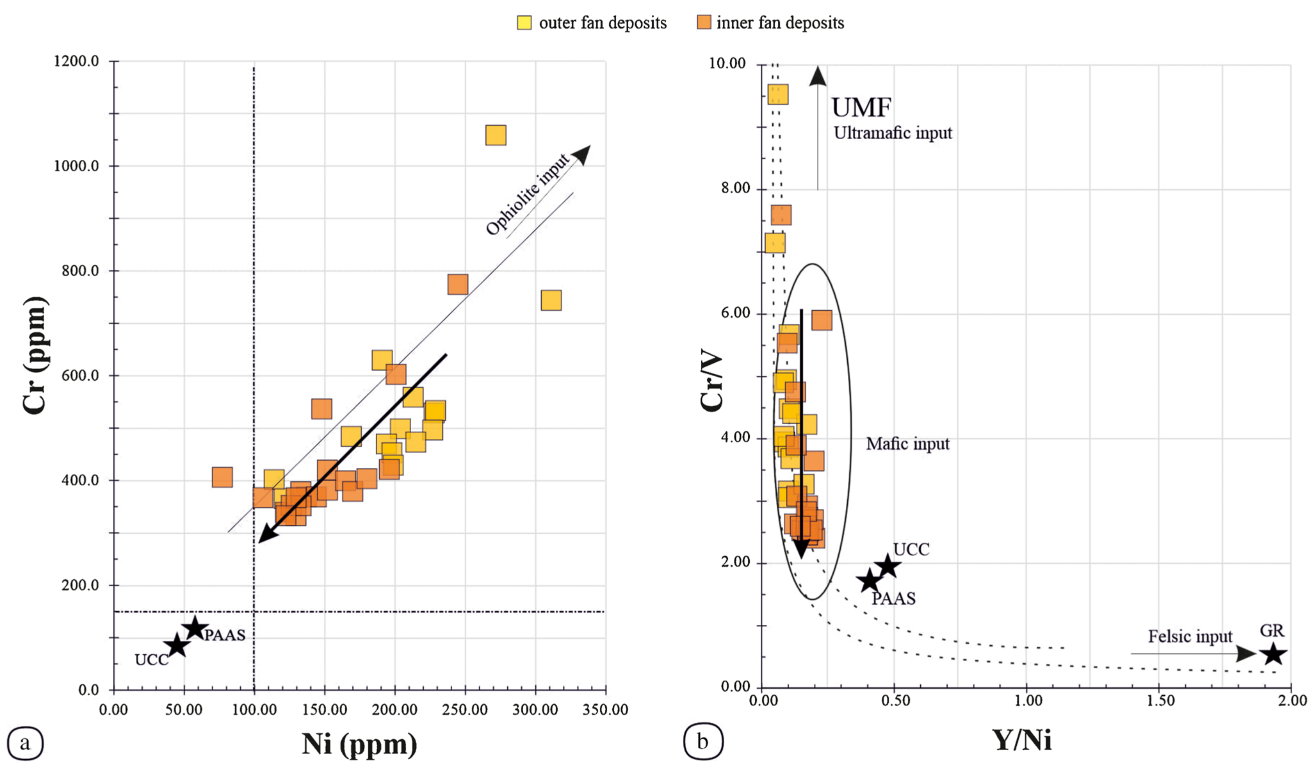

Fig. 15 Discrimination plots of (**a**) Ni against Cr after Garver et al. (1996) and (**b**) Y/Ni against Cr/V after McLennan et al. (1993). Samples that exceed the limits of 100 ppm Ni and 150 ppm Cr (dashed line) and that are enriched in the Cr/V ratio suggest mafic input. Abbreviations: PAAS: Post-Archean Australian Shale; UCC: Upper Continental Crust

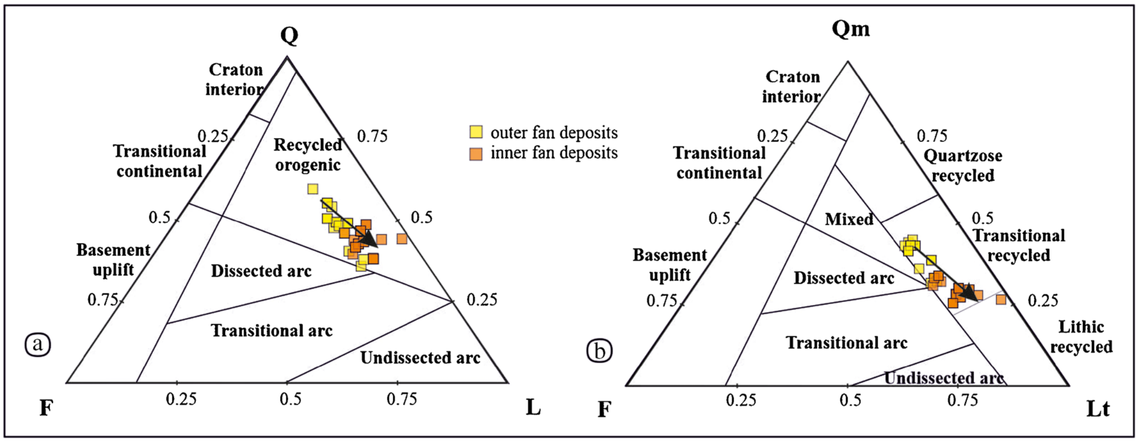

Fig. 16 Ternary diagrams (after Dickinson et al. 1983) showing provenance fields defined by (**a**) total quartz, feldspar and unstable (nonquartzose) lithic fragments; (**b**) monocrystalline quartz, feldspar and unstable lithic fragments including extrabasinal carbonate lithic fragments plus polycrystalline quartz; monocrystalline plus polycrystalline quartz, feldspar and unstable lithic fragments including extrabasinal carbonate lithic fragments plus tectonite quartz and chert. The arrow illustrates the stratigraphic upward trend of the studied thin-sections

Jurassic rifting include the pre-Apulian platform, Ionian basin, Gavrovo platform, Pindos basin, and Parnassos and Pelagonian platforms (e.g. Aubouin 1965; Smith et al. 1979; Robertson et al. 1991; Karakitsios 1995, 2013; Zelilidis et al. 2003; Bourli et al. 2019a, 2019b). The distribution of shallow limestones and dolomites in the platform belts and pelagic marine carbonates in the deeper basin reflects these formations. In the Late Cretaceous and Early Cenozoic, the convergence of Africa and Eurasia caused the collision of the Apulia microcontinent with various continental fragments (e.g., Dewey et al. 1973). This collision resulted in the inversion of Mesozoic basins and the development of the External Hellenides thrust belt (Jacobshagen et al. 1978; Skourlis and Doutsos 2003; Kaplanis et al. 2013; Chatzaras et al. 2013). The thrusting in the external Hellenides occurred sequentially from east to west (Smith and Moores 1974; Robertson and Dixon and Robertson 1984). The Parnasos and Pelagonian units migrated westward, leading to the Late Eocene thrusting of the Pindos unit on top of the Gavrovo unit, causing flexural subsidence (Fig. 18). PFB is a depocenter formed by the Pindos Orogen, characterized by high sedimentation rates associated with the nascent orogen (e.g., Aubouin 1959; Konstantopoulos and Zelilidis 2012; Botziolis et al. 2021; Kovani et al. 2023).

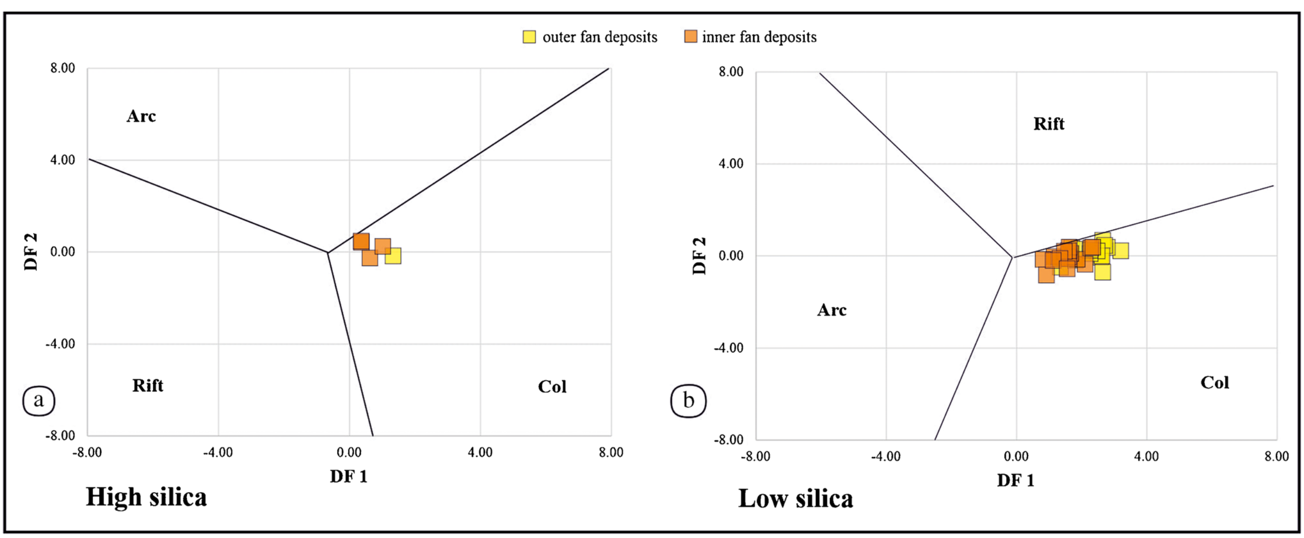

Fig. 17 Discriminant function multi-dimensional plots for both high-silica (**a**) and low-silica (**b**) clastic sediments (after Verma and Armstrong-Altrin 2013)

The Pindos Orogen includes a variety of units that have been involved in the sedimentation of PFB. The Pelagonian unit consists of Variscan basement, unconformably overlain by an Early to Middle Triassic sedimentary succession that consists of sandstone, slate, schist, chert, marl, limestone, and a deformed succession of lavas (basalts, trachy-basalts, basaltic andesites, and basaltic trachy-andesites), tuffites, and welded tuffs of Early to Middle Triassic volcanism (Smith et al. 1975; Jacobshagen and Wallbrecher 1984; Pe-Piper and Panagos 1989; Smith, 1993; Pe-Piper et al. 1996; Stampfli et al. 1998; De Bono 1998; Sharp and Robertson 2006). This type of volcanism has been recorded from northern Italy to Turkey (Stampfli 1996) and may be related to an arc-related volcanism, most likely brought on by back-arc rifting (Pe-Piper 1982; Pe-Piper and Panagos 1989). Up-section, the rock units are represented by Middle Triassic to Jurassic carbonate succession followed by Lower Cretaceous conglomerates and carbonates, and finally Upper Cretaceous to Lower Eocene deep-sea fan deposits (Jacobshagen and Wallbrecher 1984). The Parnasos units are represented by a series of shallow carbonate platform deposits of Triassic to Cretaceous age (e.g. Mountrakis 1985; Pomoni-Papaioannou 1994), overlain by deep-sea fan deposits of Palaeocene to Eocene age. The Pindos older rocks units are Middle to Upper Triassic sandstone, chert, marl, limestone, and volcano-sedimentary material (Aubouin 1957; Aubouin et al. 1970; Wagreich et al. 1996). Up-section, Upper Triassic to Lower Jurassic mudstone, sandstone, siliceous limestone, and chest are followed by Middle to Upper Jurassic multicoloured cherts with thin layers of clayey-siliceous material, pellites, and limestone. Up-section, Upper Jurassic to Lower Cretaceous limestones with thin layers of clayey-marly material and cherts, as well as brecciated limestones, calc-limestones, and cherts, are followed by Lower Cretaceous

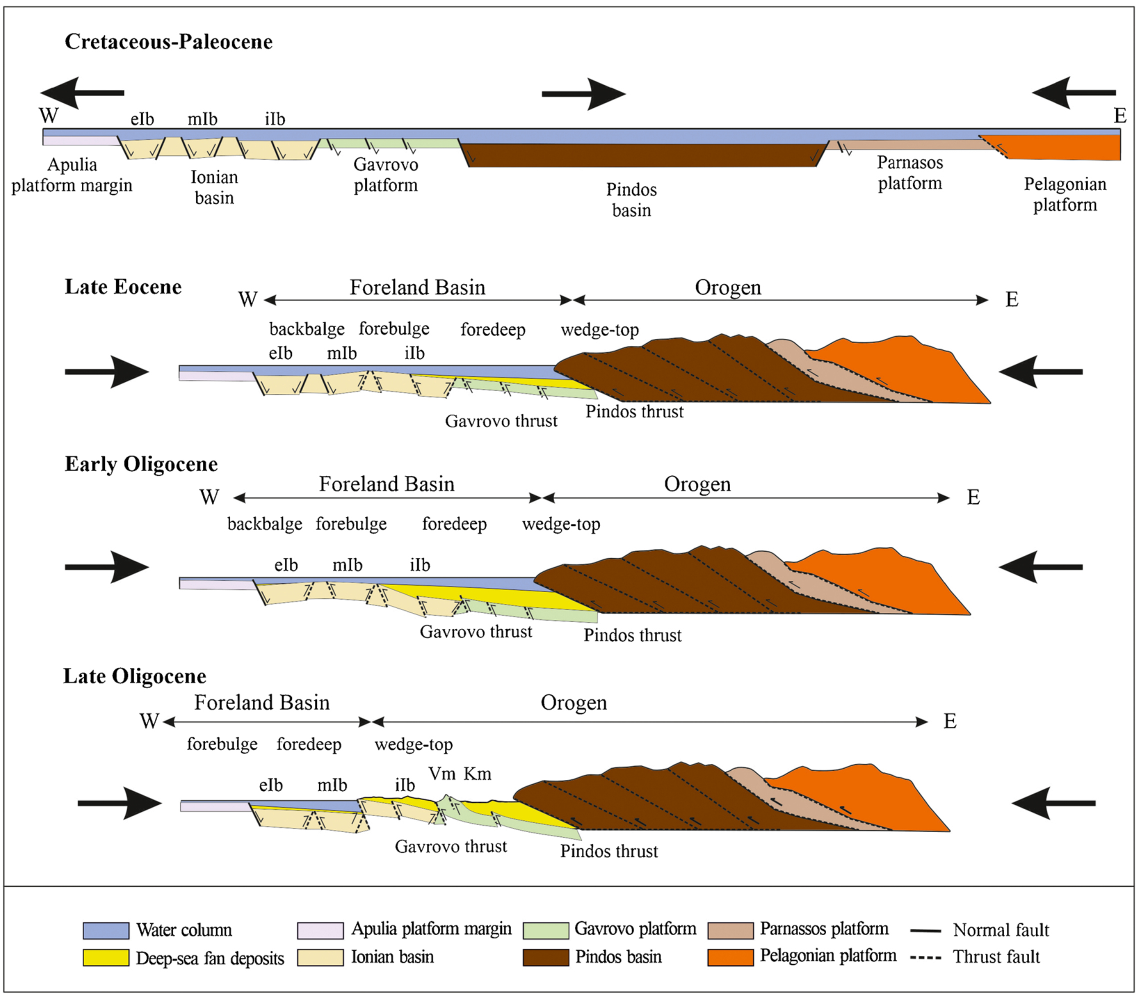

Fig. 18 Evolutionary model of the external Hellinides during the Cretaceous–Lower Eocene extension (rifting period) and Lower Eocene-Oligocene compression (modified from Bourli et al. 2019a, 2022; Botziolis et al. 2021; Zoumpouli et al. 2022). Notice the gradual westward migration of the Pindos orogen. Abbreviations: eIb = external Ionian basin; mIb = middle Ionian basin; iIb = internal Ionian basin; Vm = Varasova mountain; Km = Klokova mountain

limestones with cherts, and a series of Upper Cretaceous to Lower Eocene transitional beds composed of mudstone, sandstone, and limestones. The Pindos youngest rock units are the Upper Eocene to Late Pliocene submarine-fan deposits (Fleury 1980; Ananiadis et al. 2004).

Sedimentation can be influenced by both uplift and erosion occurring simultaneously at different source locations, with the erosion of quickly uplifted sediments resulting in enormous volumes of debris that can travel hundreds of kilometres (Critelli 1993; Ingersoll et al. 2003; Garzanti et al. 2004a, 2004b). Each source may influence sediments composition by directly supplying detritus to the basins in an axial or longitudinal sediment delivery network and by reworking other sedimentary basins that are part of the same system, as they become part of the growing orogen prior to deposition in the developing foreland basin. The detrital signatures of the sediments may change over time because of two factors: (a) the progressive lateral growth of the external belts that shields the foreland basin from receiving detritus from the axial belt, and (b) the fluctuation along the basin of the entry points of the main draining system of the axial belt (Muttoni et al. 2003; Najman et al. 2003). Transit distance, the impact of strike-slip fault zones, and sediment distribution techniques are other elements influencing this trend (direct against longitudinal transport) (Schwab 1981).

Sediment deposition in the PFB is thought to be influenced by the Pindos Orogen thrust system and the related strike-slip faults (Zelilidis et al. 2008). The Pindos Orogen was the main source of sediment, according to the paleocurrent analysis, which shows a paleodispersal direction (NE-SW) axial to it (Botziolis et al. 2021). The quartz and low feldspar contents of the sandstones indicate that these sediments were likely generated by large rivers from collision orogen and foreland uplift sources (Dickinson and Suczek 1979). In the Pindos thrust zone, coarse-grained deposits (conglomeratic channels) have been found, and they are strongly connected to transform fault zones that crosscut the thrust (Fig. 19). This connection demonstrates that these faults acted as entrance points (Figs. 19, 20). The Pindos drainage system entering the basin quickly shifted to axial direction flows (because of its geometry) and channels were formed supplying and delivering the debris from the Pindos orogen source regions, depositing the sand-rich lobe system (Fig. 20).

The potential source rocks that contributed to the PFB sedimentation were identified by the mineral composition of the studied sandstones. Non-undulatory monocrystalline quartz grains and polycrystalline quartz (with < 5 splits) may have originated from tonalites found in Middle to Late Triassic volcanic-sedimentary strata of the Pelagonian unit. Moreover, PFB sandstone contains both plagioclase, feldspar, and alkali feldspar, although plagioclase is more prevalent. The presence of plagioclase, feldspar and alkali feldspar in sandstone can be indicative of a volcanic origin. Plagioclase and feldspar are typically more abundant in volcanic rocks compared to alkali feldspar. Therefore, as plagioclase is more prevalent in the PFB sandstone, it suggests a volcanic origin, most likely from a source rock related to the Early to Middle Triassic volcanic units (granite-tonalite rock) of the Pelagonian unit. These findings are consistent with sedimentation in a pro-foreland basin, which is distinguished by the presence of (recycled) sedimentary material from shallow crustal depth sources (Nagel et al. 2014). Polycrystalline quartz (with > 5 splits) and undulatory quartz grains were sourced from low grade metamorphic rocks and earlier sandstone provenances (Folk 1974; Basu et al. 1975), thus, can be ascribed to the sandstone, slate, and schist succession of the Middle to Upper Triassic formation of the Pelagonian and Pindos units, as well as the Upper Cretaceous to Lower Eocene mudstone and sandstone of Pindos unit. This interpretation is further suggested by the sandstone, slate and schist fragments, as well as by the presence of detrital chlorite in the thin sections. Sandstone source rocks include the Upper Cretaceous to Lower Eocene deep-sea fan deposits of Pelagonian units, the Palaeocene to Eocene deep-sea fan deposits of Parnasos units, and the Upper Eocene to Lower Pliocene submarine-fan deposits of Pindos units. The Middle to Upper Triassic chert beds, Upper Triassic to Upper Jurassic multi-coloured chert beds, and Upper Jurassic to Upper Cretaceous limestones that contain cherts are probable Pindos units that could have provided chert in PFB.

Following the sandstone petrography, the geochemical analysis confirms that the studied sedimentary rocks were deposited in a collisional setting and that the PFB sediments were derived from a variety of rock types, including felsic to intermediate volcanic, sedimentary, and low-grade metamorphic rocks. Geochemical analyses of volcanic rocks from the Pelagonian unit, using rock/MORB and rock/chondrite REE spider diagrams and K_2O-SiO_2, N_2O+K_2O-SiO_2, Ti-Zr-Y, Ti-Zr scatter diagrams reveal calc-alkaline to alkaline affinities (De Bono 1998; De Bono et al. 1998, 1999), similar to the studied sediments, further supporting the petrographical interpretation. Despite the absence of mafic minerals, the elevated Ni and Cr levels of the samples indicate that the Pindos ophiolite complexes also contributed detritus in the PFB. The stratigraphic location of the samples with the highest Ni, Cr, and V concentrations is shown in Fig. 4, indicating that the predominant contribution from a mafic source occurs in the upper-part of the outer fan deposits, above the Eocene-Oligocene boundary. The Jurassic Pindos Ophiolite complex in western Greece is a supra-subduction ophiolite with lavas and cross-cutting dykes representing a diverse spectrum of magma types (Dupuy et al. 1984; Pearce et al. 1984; Kostopoulos and Murton 1992; Pe-Piper et al. 2004). These rocks, which range in composition from high-Ti mid-ocean ridge basalt (MORB) to island-arc tholeiites (IAT)

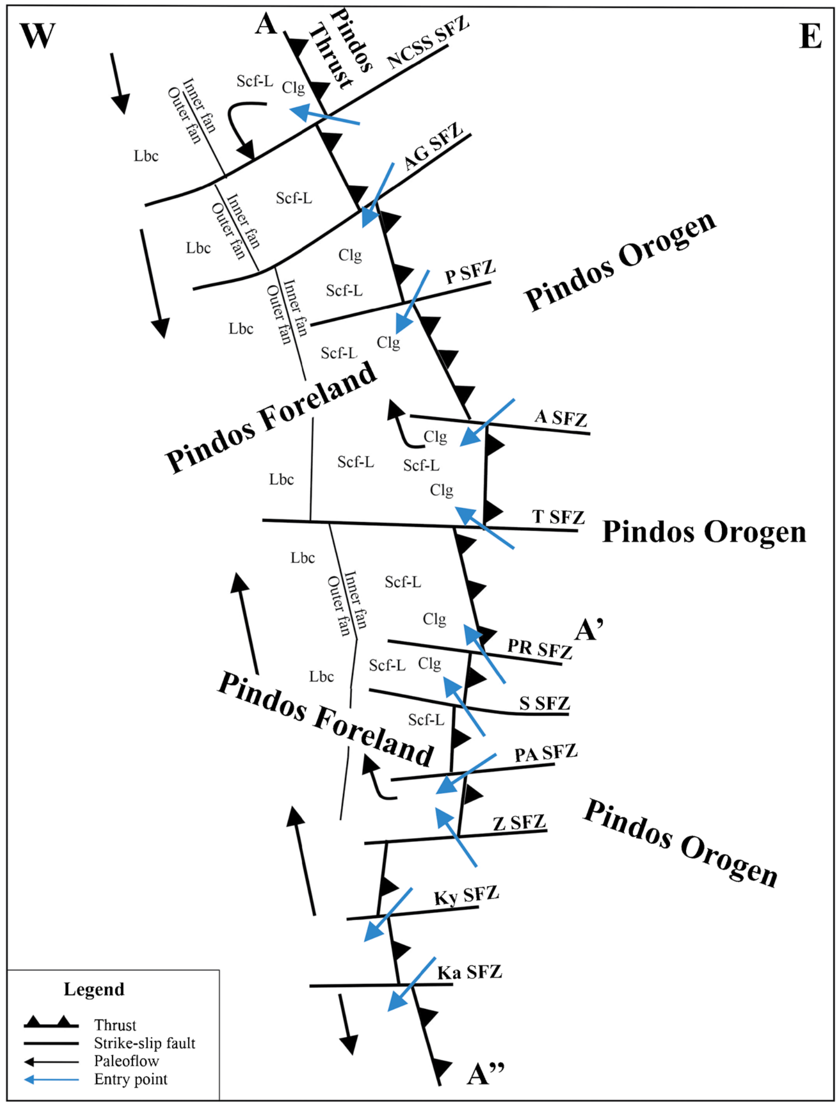

Fig. 19 Schematic diagram (check Fig. 1 for the A-A'-A" cross section profile) illustrating the proposed entry points of the sediments into the basin. Abbreviations: Clg = Conglomeratic channels; Scf-L = Sandy channels and levees; Lbs = lobe-axis, lobe off-axis, lobe fringe and distal lobe fringe; NCSS SFZ = North Corfu–South Salento strike-slip fault zone; AG SFZ = Agia Kiriaki strike-slip fault zone; P SFZ = Paramithia strike-slip fault zone; A SFZ = Alevrada strike-slip fault zone; T SFZ = Lake Trichonis strike-slip fault zone; PR SFZ = Patra-Rio strike-slip fault zone; S SFZ = Simopoulo strike-slip fault zone; PA SFZ = Pyrgos-Alfeios strike-slip fault zone; Z SFZ = Zacharo strike-slip fault zone; Ky SFZ = Kyparissia strike-slip fault zone; Ka SFZ = Kalamata strike-slip fault zone

to boninites, are probable source rocks, explaining the high to extremely high Cr and Ni levels found in these samples. The lack of mafic minerals observed in the thin sections may be attributed to their transformation into secondary minerals, such as chlorite or carbonates. Consequently, Cr and Ni could potentially reside within these secondary minerals formed because of alteration of primary minerals. It is also conceivable that Cr and Ni are contained in fine-grained minerals that are not readily discernible through microscopic analysis under a polar microscope.

Sandstone composition can also give information about the sediment source and the unroofing history of the orogen, reflecting geographical and temporal variations of erosion. Detritus from the volcanic arc and subduction complex is present in the early phases of basin formation (Dorsey 1988; Garzanti et al. 1996; Najman and Garzanti 2000). The input of metamorphic debris steadily increases as the axial metamorphic core of the orogen expands during later collisional stages (White et al. 2002). At the early stage of the orogenic evolution, the PFB fills with sediments originating from the Pelagonian units as evidenced by the high proportion of monocrystalline and polycrystalline quartz (<5 grain splits), indicating a dominant igneous source rock. The up-section increase in the abundance of quartz with undulose extinction and/or having >5 grain splits, chert, sandstone and low-grade metamorphic lithic fragments (slate, and schist) are most likely associated with the progressive unroofing of the Pindos orogen. This tendency of temporal increase in lithic fragments throughout compositional transitions, marks the shift from stable craton (Pelagonian unit) to orogen (Pindos unit) and indicates the westwards migration of the Pindos orogen. At this later collisional stage, the contribution of the exposed metamorphic and sedimentary rocks of the orogenic axial core prevails (Parnasos and Pindos units), as indicated by the increase in lithic fragments and the decreasingly contribution of the igneous source rock (Pelagonian unit)

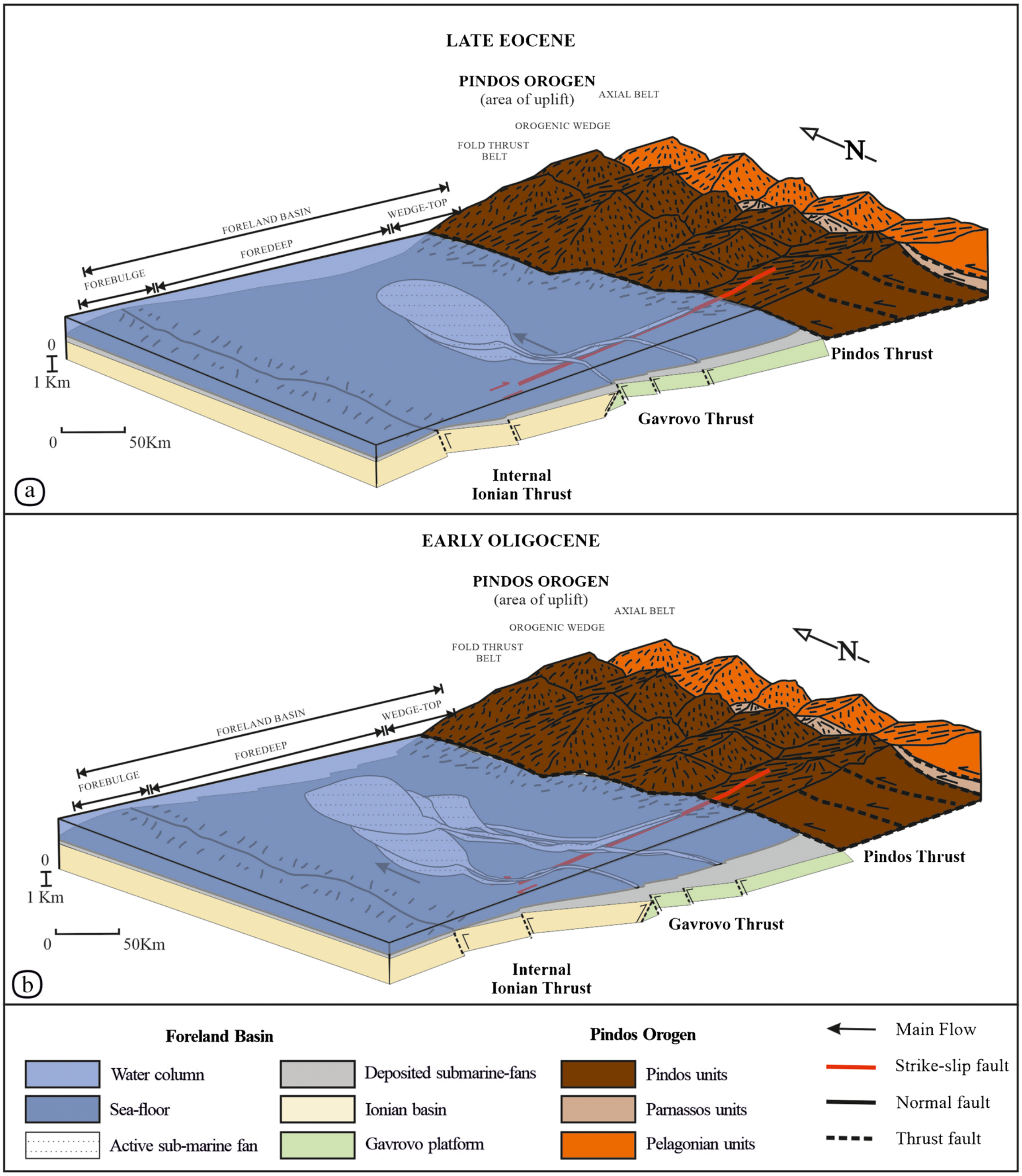

Fig. 20 3D model reconstruction illustrating the depositional setting of the Pindos Foreland Basin during the (**a**) Late Eocene and (**b**) Early Oligocene

is indicated by the decreasing trend of feldspathic, volcanic lithic, and monocrystalline quartz. This "shielding" can be further confirmed by the Cr vs Ni and Cr/V vs Y/Ni plots (Fig. 15a, b) that document a progressive upward decrease in the involvement of mafic rocks as a contributor to the basin sedimentation.

According to Kovani et al. (2023), provenance analyses of the conglomeratic matrix within the submarine fan deposits in the PFB have revealed similar trends. These trends have been interpreted as being influenced by the growth of the Pindos Orogen. Additionally, the progressive unroofing of the Himalaya Orogen throughout the Paleogene is demonstrated by an increase in the proportion of monocrystalline quartz and total lithic fragments from the lower Rud Faqirzai formation to the overlying Manzaki formation (Qayyum et al. 2001). On another example, the Sierra de Reyes foreland basin displays similar trends and indicates a typical unroofing history that resulted in the deposition of a succession with variable clastic composition, followed by an up-section enrichment in metamorphic rock fragments (Sagripanti et al. 2012). As a result, the detrital patterns of the deposited submarine fans in foreland basins collectively document the gradual unroofing of the orogen in a chronological and geographical context.

Conclusions

Petrographic and geochemical data, combined with previous sedimentological and stratigraphic analyses of the examined deposits, have provided insights into the PFB provenance and tectonic setting. The geochemical and petrographic composition of the sediments is principally affected by the different exhumation history of the source rocks and the distance of transportation. Petrographic analysis of sandstones revealed that PFB samples contain debris derived mostly from sedimentary and low-grade metamorphic rocks of the Pindos Orogen. The sedimentary sequence exhibits a general upward enrichment in sedimentary and metamorphic lithic fragments, as well as an upward reduction in monocrystalline quartz grains, feldspathic, and volcanic lithic clasts associated with the unroofing of the Pindos Orogen. The rapid exhumation of Pindos Orogen strata is demonstrated by the increasing trend in the quantity of lithic fragments in sedimentary layers, which is related with the Pindos Orogen's unroofing and rapid uplift rates.

The samples are geochemically immature and originated from a source with a low to moderate degree of weathering, according to the ICV and CIA values. The PFB's sediments exhibit PAAS-like chemical properties and are hence derived from a differentiated UCC. The Pindos orogen supplied sediments with calc-alkaline to alkaline affinities. The trace and REE concentrations in the samples, as well as the trace element ratios, revealed that the debris originated mostly from felsic to intermediate rocks, with a minor contribution from a mafic source. The formations exhibit PAAS-like affinities but are depleted in Si_2O, Zr and Hf compared to PAAS, suggesting that they are generated from differentiated UCC, with low recycle. The Early to Middle Triassic volcanic rocks, the Upper to Lower Cretaceous carboniferous and radiolarite formations, and the Paleocene submarine-fan deposits, as well as the ophiolite complexes of the Pindos Orogen, are potential sources of detritus.

Based on the QFL and QmFLt ternary plots, the sedimentary rocks from the PFB originated from a recycled orogen. Multidimensional discrimination diagrams suggest sediment sources from a collisional setting and confirm the active continental margin setting. This explanation is in agreement with the geology of the PFB and is linked to the collision of the Apulia and Eurasian plates, which resulted in the development of the Alpine orogen. It is deduced that the studied area served as a foreland basin attached to the growing orogeny resulting from the continental collision.

Supplementary Information The online version contains supplementary material available at https://doi.org/10.1007/s12517-023-11586-9.

Acknowledgements Thanks to the journal editor in chief (Prof. Abdullah M. Al-Amri), the reviewer Prof. Salvatore Critelli and the anonymous reviewer for their constructive criticism that greatly improved the manuscript.

Funding This work was funded by the H.F.R.I. (Hellenic Foundation for Research and Innovation) and G.S.R.T. (General Secretarial for Research and Technology) through the research project "Global climate and sea-level changes across the Latest Eocene-Early Oligocene, as reflected in the sedimentary record of Pindos foreland and Thrace basin, Greece, 80591".

Data Availability The data used in this study are provided in the Supplementary Material of this article.

Declarations

Conflict of interest The authors declare that they have no competing interests.

References

Ali S, Stattegger K, Garbe-Schönberg D, Frank M, Kraft S, Kuhnt W (2014) The provenance of Cretaceous to Quaternary sediments in the Tarfaya basin, SW Morocco: evidence from trace element geochemistry and radiogenic Nd-Sr isotopes. J Afr Earth Sci 90:64–76. https://doi.org/10.1016/j.jafrearsci.2013.11.010

Amendola U, Perri F, Critelli S, Monaco P, Cirilli S, Trecci T, Rettori R (2016) Composition and provenance of the Macigno Formation (Late Oligocene-Early Miocene) in the Trasimeno Lake area (Northern Apennines). Mar Pet Geol 69:146–167

Ananiadis G, Vakalas I, Zelilidis A, Stoykova K (2004) Paleographic evolution of Pindos basin during Paleogene using calcareous nannofossils. Bull Geol Soc Greece 36(2):836–845

Armstrong-Altrin JS, Machain-Castillo ML, Rosales-Hoz L, Carranza-Edwards A, Sanchez-Cabeza JA, Ruíz-Fernández AC (2015) Provenance and depositional history of continental slope sediments in the Southwestern Gulf of Mexico unraveled by geochemical analysis. Cont Shelf Res 95:15–26. https://doi.org/10.1016/j.csr.2015.01.003

Armstrong-Altrin JS, Nagarayan R, Lee YI, Zubillaga JJK, Saldana LPC (2014) Geochemistry of sands along the San Nicolás and San Carlos beaches, Gulf of California, Mexico: implications for provenance and tectonic setting. Turk J Earth Sci 23(5). https://doi.org/10.3906/yer-1309-21

Aubouin J (1957) Essai de correlations stratigraphiques en Grece occidentale. Bulletin de la Société Géologique de France (1957) S6-VII (4-5):281–304. https://doi.org/10.2113/gssgfbull.S6-VII.4-5.281

Aubouin J (1959) Contribution a l'etudegeologique de la Greceseptrionale: les confins de 1'Epire et de la Thessalie. Ann Geol Pays Helleniques 9:279–295

Aubouin J (1965) Geosynclines, Development in Geotectonics. Elsevier

Aubouin J, Blanchet R, Cadet JP, Celet P, Chavret J, Chorowics J, Cousin M, Rampnoux JP (1970) Contribution a la geologic des

Hellenides: le Gavrovo, le Pinde et la zone ophiolitique subpelagonienne. Ann Sot Geol Nord 90:277–306

Avramidis P, Zelilidis A (2001) The nature of deep-marine sedimentation and palaeocurrent trends as an evidence of Pindos foreland basin fill conditions. E24 No4:252–256. https://doi.org/10.18814/epiiugs/2001/v24i4/005

Avramidis P, Zelilidis A, Kontopoulos N (2000) Thrust dissection control of deepwater clastic dispersal patterns in the Klematia-Paramythia Foreland Basin, Western Greece. Geol Mag 137:667–685. https://doi.org/10.1017/S0016756800004684

Barth M, McDonough WF, Rudnick RL (2000) Tracking the budget of Nb and Ta in the continental crust.Chem Geol 165(3–4):197–213.https://doi.org/10.1016/S0009-2541(99)00173-4

Basu A, Young SW, Suttner LJ, James WC, Mack GH (1975) Re-evaluation of the use of undulatory extinction and polycrystallinity in detrital quartz for provenance interpretation. J Sediment Res 45(4):873–882. https://doi.org/10.1306/212F6E6F-2B24-11D7-8648000102C1865D

Bauluz B, Mayayo MJ, Fernandez-Nieto C, Gonzalez Lopez JM (2000) Geochemistry of Precambrian and Paleozoic siliciclastic rocks from the Iberian Range (NE Spain): implications for source-area weathering, sorting, provenance, and tectonic setting. Chem Geol 168:135–150. https://doi.org/10.1016/S0009-2541(00)00192-3

Beaumont C (1981) Foreland basins. Geophys J Int 65(2):291–329. https://doi.org/10.1016/0040-1951(94)00123-Q

Bega Z (2015) Hydrocarbon exploration potential of Montenegro - a brief review. J Pet Geol 38(3):317–330. https://doi.org/10.1111/jpg.12613

Bhatia MR (1985) Rare-earth element geochemistry of Australian Paleozoic Graywackes and Mudrocks: provenance and tectonic control. Sediment Geol 45:97–113. https://doi.org/10.1016/0037-0738(85)90025-9

Bock B, McLennan SM, Hanson GN (1998) Geochemistry and provenance of the Middle Ordovician Austin Glen Member (Normanskill Formation) and the Taconian Orogeny in New England. Sedimentology 45:635–655. https://doi.org/10.1046/j.1365-3091.1998.00168.x

Boggs S, Kwon YI, Goles GG, Rusk BG, Krinsley D, Seyedolali A (2002) Is quartz cathodoluminescence color a reliable provenance tool? A quantitative examination. J Sediment Res 72(3):408–415. https://doi.org/10.1306/102501720408

Botziolis C, Maravelis AG, Pantopoulos G, Kostopoulou S, Catuneanu O, Zelilidis A (2021) Stratigraphic and paleogeographic development of a deep-marine foredeep: Central Pindos foreland basin, western Greece. Mar Pet Geol 128. https://doi.org/10.1016/j.marpetgeo.2021.105012

Bourli N, Iliopoulos G, Zelilidis A (2022) Reassessing depositional conditions of the pre-apulian zone based on synsedimentary deformation structures during Upper Paleocene to Lower Miocene carbonate sedimentation, from Paxoi and Anti-Paxoi Islands, Northwestern End of Greece. Minerals 12:201. https://doi.org/10.3390/min12020201

Bourli N, Kokkaliari M, Iliopoulos I, Pe-Piper G, Piper DJW, Maravelis AG, Zelilidis A (2019b) Mineralogy of siliceous concretions, Cretaceous of Ionian zone, western Greece: implication for diagenesis and porosity. Mar Pet Geol 105:45–63

Bourli N, Pantopoulos G, Maravelis AG, Zoumpoulis E, Iliopoulos G, Pomoni-Papaioannou F, Kostopoulou S, Zelilidis A (2019a) Late Cretaceous to Early Eocene geological history of the eastern Ionian Basin, southwestern Greece: an integrated sedimentological and bed thickness statistics analysis. Cretac Res 98:47–71

Cantalamessa G, Di Celma C (2004) Sequence response to syndepositional regional uplift: insights from high-resolution sequence stratigraphy of late Early Pleistocene strata, Periadriatic Basin, central Italy. Sediment Geol 164:283–309

Catuneanu O (2004) Basement control on flexural profiles and the distribution of foreland facies: The Dwyka Group of the Karoo Basin, South Africa. Geology 32:517–520

Catuneanu O (2018) First-order foreland cycles: interplay of flexural tectonics, dynamic loading, and sedimentation. J Geodyn. https://doi.org/10.1016/j.jog.2018.03.001

Chatzaras V, Xypolias P, Kokkalas S, Koukouvelas I (2013) Tectonic evolution of a crustal-scale oblique ramp, Hellenides thrust belt, Greece. J Struct Geol 57:16–37. https://doi.org/10.1016/j.jsg.2013.10.003

Chen M, Sun M, Cai K, Buslov MM, Zhao G, Rubanova ES (2014) Geochemical study of the Cambrian-Ordovician meta-sedimentary rocks from the Altai-Mongolian terrane, northwestern Central Asian Orogenic Belt: implications on the provenance and tectonic setting. J Asian Earth Sci 96:69–83. https://doi.org/10.1016/j.jseaes.2014.08.028

Chen WS, Ridgway KD, Horng CS, Chen YG, Shea KS, Yeh MG (2001) Stratigraphic architecture, magnetostratigraphy and incised-valley systems of the Pliocene–Pleistocene collisional marine foreland basin Taiwan. Geol Soc Am Bull 113:1249–1271

Clews JE (1989) Structural controls on basin evolution: Neogene to Quaternary of the Ionian zone, Western Greece. J Geol Soc 146(3):447–457

Condie KC (1993) Chemical composition and evolution of the Upper Continental Crust; contrasting results from surface samples and shales. Chem Geol 104:1–37. https://doi.org/10.1016/0009-2541(93)90140-E

Cox R, Lowe DR, Cullers R (1995) The influence of sediment recycling and basement composition on evolution of mudrock chemistry in the southwestern United States. Geochimica et Cosmochimica Acta 59:2919–2940. https://doi.org/10.1016/0016-7037(95)00185-9

Critelli S (1993) Sandstone detrital modes in the Paleogene Liguride Complex, accretionary wedge of the Southern Apennines (Italy). J Sediment Petrol 63:464–476

Critelli S (2018) Provenance of Mesozoic to Cenozoic Circum-Mediterranean sandstones in relation to tectonic setting. Earth Sci Rev 185:624–648

Critelli S, Arribas J, Le Pera E, Tortosa A, Marsaglia KM, Latter KK (2003) The recycled orogenic sand provenance from an uplifted thrust-belt, Betic Cordillera, southern Spain. J Sediment Res 73:72–81

Critelli S, Criniti S (2021) Sandstone petrology and provenance in Fold Thrust Belt and Foreland Basin System. In: Sedimentary petrology - implications in petroleum industry (edited by Ali Ismail Al-Juboury). Intech Open Access Publisher, Janeza Trdine 9, Rijeka, Croatia, 1-15. https://doi.org/10.5772/intechopen.96985.

Critelli S, Martín-Martín M (2022) Provenance, paleogeographic and paleotectonic interpretations of Oligocene-Lower Miocene sandstones of the western-central Mediterranean region: a review. In: "The evolution of the Tethyan orogenic belt and, related mantle dynamics and ore deposits". J Asian Earth Sci Special Issue X8:100124. https://doi.org/10.1016/j.jaesx.2022.100124

Cullers RL (1994) The chemical signature of source rocks in size fractions of Holocene stream sediment derived from metamorphic rocks in the Wet Mountains region, USA. Chem Geol 113:327–343. https://doi.org/10.1016/0009-2541(94)90074-4

Cullers RL (2000) The geochemistry of shales, siltstones, and sandstones of Pennsylvanian-Permian age. Colourado, USA: implications for provenance and metamorphic studies. Lithos 51:181–203

Cullers RL, Podkovyrov VN (2000) Geochemistry of the Mesoproterozoic Lakhanda shales in southeastern Yakutia, Russia: implications for mineralogical and provenance control, and recycling. Precambrian Res 104:77–93. https://doi.org/10.1016/S0301-9268(00)00090-5

De Bono A, Vavassis I, Stampfli GM, Martini R, Vachard D, Zaninetti L (1999) New stratigraphic data on the Pelagonian pre-Jurassic units of Evia island, (Greece). Ann Geol Pays Hellen 38:11–24

De Bono A (1998) Pelagonian margins in central Evia island (Greece). Stratigraphy and geodynamic evolution. Thèse de doctorat, Université de Lausanne, p 114

De Bono A, Vavassis I, Stampili GM (1998) A Triassic flysch sequence in the Pelagonian realm of Evia island (Greece), Proc. of the VIII International Congress of the Geological Society of Greece

De Graciansky PC, De Dardeau G, Lemoine M, Tricart P (1989) The inverted margin of the French Alps. Geol Soc, London, SPubl 44(1):87–104. https://doi.org/10.1144/GSL.SP.1989.044.01.06

Deer WA, Howie RA, Zussman J (2013) Chlorite Group: clinochlore (Mg)10Al2[Al2Si6O20](OH)16 - Chamosite (Fe2+)10Al2[Al2Si6O20](OH)16 in Deer WA. In: Howie RA, Zussman J (eds) An introduction to the rock-forming minerals. Mineralogical Society of Great Britain and Ireland

Degnan PJ, Robertson AHF (1998) Mesozoic–early Tertiary passive margin evolution of the Pindos Ocean (NW Peloponnese, Greece). Sed Geol 117:33–70. https://doi.org/10.1016/S0037-0738(97)00113-9

Dewey JF, Pitman WC, Ryan WBF, Bonnin J (1973) Plate tectonics and the evolution of the Alpine System. GSA Bull 84(10):3137–3180. https://doi.org/10.1130/0016-7606(1973)84<3137:PTATEO>2.0.CO;2

Dickinson WR (1970) Interpreting detrital modes of graywacke and arkose. J Sediment Res 40(2):695–707. https://doi.org/10.1306/74D72018-2B21-11D7-8648000102C1865D

Dickinson WR, Beard LS, Brakenridge GR, Erjavec JL, Ferguson RC, Inman KF, Knepp RA, Lindberg FA, Ryberg PT (1983) Provenance of North American Phanerozoic sandstones in relation to tectonic setting. Geol Soc Am Bull 94:222–235

Dickinson WR, Suczek DCA (1979) Plate tectonics and sandstone compositions. Am Assoc Petroleum Geologists Bull 63:2164–2182

Ding L, Kapp P, Wan X (2005) Paleocene-Eocene record of ophiolite obduction and initial India-Asia collision, south central Tibet. Tectonics 24:TC3001

Dixon JE, Robertson AHF (eds) (1984) The geological evolution of the Eastern Mediterranean. Geological Society Special Publication no. 17. vii 824 pOxford, London, Edinburgh, Boston, Palo Alto, Melbourne: Blackwell Scientific. Geol Mag 122(5):575–575. https://doi.org/10.1017/S0016756800035561

Dorsey RJ (1988) Provenance evolution and unroofing history of a modern arc-continent collision: evidence from petrography of Plio-Pleistocene sandstones, eastern Taiwan. J Sediment Petrol 58:208–218. https://doi.org/10.1306/212F8D5A-2B24-11D7-8648000102C1865D

Doutsos T, Koukouvelas I (1998) Fractal analysis of normal faults in northwestern Aegean area, Greece. J Geodyn 26:197–216

Doutsos T, Koukouvelas I, Poulimenos G, Kokkalas S, Xypolias P, Skourlis K (2000) An exhumation model of the south Peloponnesus, Greece. Int J Earth Sci 89:350–365

Doutsos T, Koukouvelas IK, Xypolias P (2006) A new orogenic model for the External Hellenides. Geol Soc, London, Spec Publ 260(1):507–520. https://doi.org/10.1144/GSL.SP.2006.260.01.21

Doutsos T, Piper G, Boronkay K, Koukouvelas I (1993) Kinematics of the Central Hellenides. Tectonics 12:936–953. https://doi.org/10.1029/93TC00108

Dupuy C, Dostal J, Capedri S, Venturelli G (1984) Geochemistry and petrogenesis of ophiolites from Northern Pindos (Greece). Bull Volcanol 47:39–46

Etemad-Saeed N, Hosseini-Barzi M, Armstrong-Altrin JS (2011) Petrography and geochemistry of clastic sedimentary rocks as evidences for provenance of the Lower Cambrian Lalun Formation, Posht-e-badam block, Central Iran. J Afr Earth Sci 61(2):142–159.

Etemad-Saeed N, Hosseini-Barzi M, Edabi MH, Sadeghil A, Houshmandzadeh A (2015) Provenance of Neoproterozoic sedimentary basement of northern Iran, Kahar Formation. J African Earth Sci 111:54–75. https://doi.org/10.1016/j.jafrearsci.2015.07.003

Fathy D, Wagreich M, Zaki R, Mohamed RSA, Gier S (2018) Geochemical fingerprinting of Maastrichtian oil shales from the Central Eastern Desert, Egypt: implications for provenance, tectonic setting, and source area weathering. Geol J 53(6):2597–2612. https://doi.org/10.1002/gj.3094

Faupl P, Pavlopoulos A, Migiros G (1998) On the provenance of flysch deposits in the External Hellinides of mainland Greece: results from heavy minerals studies. Geol Mag 135:421–442. https://doi.org/10.1017/S001675689800870X

Fedo CM, Eriksson KA, Krogstad EJ (1996) Geochemistry of shales from the Archean (~3.0 Ga) Buhwa Greenstone Belt, Zimbabwe: implications for provenance and source-area weathering. Geochimica et Cosmochimica Acta 60(10):1751–1763. https://doi.org/10.1016/0016-7037(96)00058-0

Fedo CM, Nesbitt HW, Young GM (1995) Unraveling the effects of potassium metasomatism in sedimentary rocks and paleosols, with implications for paleoweathering conditions and provenance. Geology 23:921–924. https://doi.org/10.1130/0091-7613(1995)023<0921:UTEOPM>2.3.CO;2

Fleury JJ (1980) Les zones de Gavrovo-Tripolitza et du Pinde-Olonus (Grèce occidentale et Péloponnese du Nord): evolution d'une plateforme et d'une bassin dans leur cadre alpin. Société Géologique du Nord 4:1–651

Floyd P, Leveridge B (1987) Tectonic environment of the Devonian Gramscatho basin, south Cornwall: framework mode and geochemical evidence from turbiditic sandstones. J Geol Soc 144:531–540. https://doi.org/10.1144/gsjgs.144.4.0531

Folk RL (1974) Petrology of Sedimentary Rocks. Hemphill Publishing Co., Austin, p 170

Frizon de Lamotte D, Raulin C, Mouchot N, Wrobel-Daveau JC, Blanpied, C, Ringenbach JC (2011) The southernmost margin of the Tethys realm during the Mesozoic and Cenozoic: Initial geometry and timing of the inversion processes. Tectonics 30:TC3002. https://doi.org/10.1029/2010TC002691

Garcia D, Coehlo J, Perrin M (1991) Fractionation between TiO2 and Zr as a measure of sorting within shale and sandstone series (northern Portugal). Eur J Mineral 3:401–414. https://doi.org/10.1127/ejm/3/2/0401

Garver JI, Royce PR, Smick TA (1996) Chromium and nickel in shale of the Taconic Foreland: a case study for the provenance of fine-grained sediments with an ultramafic source. SEPM J Sediment Res 66. https://doi.org/10.1306/D42682C5-2B26-11D7-8648000102C1865D

Garzanti E (2016) From static to dynamic provenance analysis—sedimentary petrology upgraded. Sediment Geol 336:3–13. https://doi.org/10.1016/j.sedgeo.2015.07.010

Garzanti E (2019) Petrographic classification of sand and sandstone. Earth-Sci Rev 192:545–563. https://doi.org/10.1016/j.earscirev.2018.12.014

Garzanti E, Critelli S, Ingersoll RV (1996) Paleogeographic and paleotectonic evolution of the Himalayan Range as reflected by detrital modes of Tertiary sandstones and modern sands (Indus transect, India and Pakistan). Geol Soc Am Bull 108:631–642. https://doi.org/10.1130/0016-7606(1996)108<0631:PAPEOT>2.3.CO;2

Garzanti E, Doglioni C, Vezzoli G, Ando S (2007) Orogenic belts and orogenic sediment provenance. J Geol 115:315–333. https://doi.org/10.1086/512755

Garzanti E, Padoan M, Setti M, Najman Y, Peruta L, Villa IM (2013) Weathering geochemistry and Sr-Nd fingerprints of equatorial upper Nile and Congo muds. Geochem Geophys Geosyst 14(2):292–316. https://doi.org/10.1002/ggge.20060

Garzanti E, Resentini A (2015) Provenance control on chemical indices of weathering (Taiwan river sands). Sediment Geol 336:81–95. https://doi.org/10.1016/j.sedgeo.2015.06.013

Garzanti E, Vezzoli G, Ando S, France-Lanord C, Singh SK, Foster G (2004a) Sediment composition and focused erosion in collision orogens: the Brahmaputra case. Earth Planet Sci Lett 220:157–174. https://doi.org/10.1016/S0012-821X(04)00035-4

Garzanti E, Vezzoli G, Andò S, Paparella P, Clift PD (2005) Petrology of Indus River sands: a key to interpret erosion history of the Western Himalayan Syntaxis. Earth Planet Sci Lett 229:287–302

Garzanti E, Vezzoli G, Lombardo B, Ando S, Mauri E, Monguzzi S, Russo M (2004b) Collision-orogen provenance (western and central Alps): detrital signatures and unroofing trends. J Geol 112:145–164. https://doi.org/10.1086/381655

Ghazi S, Mountney NP (2011) Petrography and provenance of the Early Permian Fluvial Warchha Sandstone, Salt Range, Pakistan. Sediment Geol 233(1–4):88–110. https://doi.org/10.1016/j.sedgeo.2010.10.013

Götze J, Zimmerle W (2000) Quartz and silica as guide to provenance in sediments and sedimentary rocks. Contrib Sediment Geol 12:91

Grosch EG, Bisnath A, Frimmel HE, Board WS (2007) Geochemistry and tectonic setting of mafic rocks in western Dronning Maud Land, East Antarctica: implications for the geodynamic evolution of the Proterozoic Maud Belt. J Geol Soc 164(00167649):465–475

Harper GD (1980) The Josephine Ophiolite—Remains of a Late Jurassic marginal basin in northwestern California. Geology 8(7):333–337.https://doi.org/10.1130/0091-7613(1980)82.0.CO;2

Hassan S, Ishiga H, Roser BP, Dozen K, Naka T (1999) Geochemistry of Permian–Triassic shales in the Salt Range, Pakistan: implications for provenance and tectonism at the Gondwana margin, Chem Geol, 158, 3–4, 293-314, https://doi.org/10.1016/S0009-2541(99)00057-1.

Hofmann A, Bolhar R, Dirks P, Jelsma H (2003) The geochemistry of Archaean shales derived from a Mafic volcanic sequence, Belingwe greenstone belt, Zimbabwe: provenance, source area unroofing and submarine versus subaerial weathering. Geochimica et Cosmochimica Acta 67(3):421–440. https://doi.org/10.1016/S0016-7037(02)01086-4

Hu X, Garzanti E, Moore T, Raffi I (2015) Direct stratigraphic dating of India-Asia collision onset at the Selandian (middle Paleocene, 59 ± 1 ma). Geology 43:859–862

Ingersoll RV, Dickinson WR, Graham SA (2003) Remnant-ocean submarine fans: largest sedimentary systems on Earth. In Chan MA, Archer AW eds. Extreme depositional environments: mega end members in geologic time. Geol Soc Am Spec Pap 370:191–208. https://doi.org/10.1130/0-8137-2370-1.191

Iqbal S, Wagreich M, Jan IU, Kuerschner WM, Gier S, Bibi M (2019) Hot-house climate during the Triassic/Jurassic transition: the evidence of climate change from the southern hemisphere (Salt Range, Pakistan). Glob Planet Change 172:15–32. https://doi.org/10.1016/j.gloplacha.2018.09.008

Jacobshagen V (1986) Geologie von Griechenland. Beitragezur Geologie der Erde Ser., vol 19. Borntraeger, Berlin, p 363

Jacobshagen V, Dorr S, Kockel F, Kopp KO, Kowalczyk G (1978) In: Closs H, Roeder D, Schmidt K (eds) Structure and geodynamic evolution of the Aegean region. Stuttgart, Schweizerbart'sche Verlagsbuchhandlung, Alps, Apennines, Hellenides, pp 537–564

Jacobshagen V, Wallbrecher E (1984) Pre-Neogene nappe structure and metamorphism of the North Sporades and the southern Pelion peninsula. In: Dixon JE, AHF R (eds) The geological evolution of the Eastern Mediterranean. Geological Society, vol 17. Special Pubi, Oxford, Blackwell, pp 591–602

Jenkins DAL (1972) Structural development of western Greece. A.A.P.G Bull 56:128–149

Jian X, Guan P, Zhang W, Feng F (2013) Geochemistry of Mesozoic and Cenozoic sediments in the northernQaidam basin, northeastern Tibetan Plateau: Implications forprovenance and weathering. Chem Geol 360–361:74–88

Johnsson MJ (1993) The system controlling the composition of clastic sediments. In: Johnsson MJ, Basu A (eds) Processes controlling the composition of clastic sediments, vol 284. Geological Society of America, Special Paper, pp 1–19. https://doi.org/10.1130/SPE284-p1

Jones G, Robertson AHF (1991) Tectonostratigraphy and evolution of the Mesozoic Pindos ophiolite and related units, northwestern Greece. J Geol Soc London 148:261–288. https://doi.org/10.1144/gsjgs.148.2.0267

Kamberis E, Marnelis F, Loukoyannakis M, Maltezou F, Hirn A, Streamers Group (1996) Structure and deformation of the external Hellenides based on seismic data from offshore western Greece. In: Wessely G, Liebl W (eds) Oil and gas in Alpidic thrust belts and basins of Central and Eastern Europe, Eur. Ass. Geo. Eng., Spec. Publ., 5. Geological Society of London, pp 207–214

Kamberis E, Sotiropoulos S, Aximniotou O, Tsaila-Monopoli S, Ioakim C (2000) Late Cenozoic deformation of Gavrovo and Ionian zone in NW Peloponnesus (western Greece). Annali di Geofisica 43:905–919. https://doi.org/10.4401/ag-3679

Kamp PCVD, Leake BE (1985) Petrography and geochemistry of feldspathic and mafic sediments of the northeastern Pacific margin. Trans R Soc Edinb: Earth Sci 76:411–449

Kaplanis A, Koukouvelas I, Xypolias P, Kokkalas S (2013) Kinematics and ophiolite obduction in the Gerania and Helicon Mountains, central Greece. Tectonophysics 595–596:215–234. https://doi.org/10.1016/j.tecto.2012.07.014

Karakitsios V (1990) Chronologie et géométrie de l'ouverture d'un bassin et de son inversion tectonique: le bassin ionien (Epire, Grèce). Mem Sc Terre Univ P: et M. Curie, Paris, 91-4, 310 p

Karakitsios V (1995) The influence of preexisting structure and halokinesis on organic matter preservation and thrust system evolution in the Ionian basin, northwestern Greece. AAPG Bull 79:960–980. https://doi.org/10.1306/8D2B2191-171E-11D7-8645000102C1865D

Karakitsios V (2013) Western Greece and Ionian Sea petroleum systems. AAPG Bull 97(9):1567–1595. https://doi.org/10.1306/02221312113

Karakitsios V, Rigakis N (1996) New oil source rocks cut in Greek Ionian basin. Oil Gas J 94(7):56–59

King G, Sturdy D, Whitney J (1993) The landscape geometry and active tectonics of northwestern Greece. Geol Soc Am Bull 105:137–161. https://doi.org/10.1130/0016-7606(1993)105<0137:TLGAAT>2.3.CO;2

Kirstein LA, Foeken JPT, Stuart FM, Phillips RJ (2009) Cenozoic unroofing history of the Ladakh Batholith, western Himalaya, constrained by thermochronology and numerical modelling. J Geol Soc 166:667–678. https://doi.org/10.1144/0016-76492008-107

Koch KE, Nicolaus HJ (1969) Zur Geologie des Ostpindos—Flyschbeckens und seiner Umrandung: the geology of Greece for geology and subsurface research. Athens: Institute for Geology and Subsurface Research; 1969.

Konstantopoulos P, Maravelis A, Zelilidis A (2013) The implication of transfer faults in foreland basin evolution: application on Pindos Foreland Basin, West Peloponnesus, Greece. Terra Nova 25:323–336. https://doi.org/10.1111/ter.12039

Konstantopoulos P, Zelilidis A (2012) The geodynamic evolution of Pindos foreland basin in SW Greece. J Int Geosci 35:501–512. https://doi.org/10.18814/epiiugs/2012/v35i4/007

Koralay T (2010) Petrographic and geochemical characteristics of upper Miocene Tekkedag volcanics (Central Anatolia—Turkey). Chemie der Erde 70:335–351

Kostopoulos D, Murton BJ (1992) Origin and distribution of components in boninite genesis: significance of the OIB component. In: Parson LM, Murton BJ, Browning P (eds) Ophiolites and their modern oceanic analogues, vol 60. Geological Society of London, Special Publication, pp 133–154

Kovani A, Botziolis C, Maravelis AG, Pantopoulos G, Iliopoulos G, Zelilidis A (2023) Provenance and statistical analysis of the Lower Oligocene gravelly deposits in central Pindos foreland basin, western Greece: implications for orogenic build-up and unroofing. Geol J 58(1):497–521. https://doi.org/10.1002/gj.4608

Le Maitre RW (1976) The chemical variability of some common igneous rocks. J Petrol 17:589–637. https://doi.org/10.1093/petrology/17.4.589

Lee YI (2002) Provenance derived from the geochemistry of late Paleozoic–early Mesozoic mudrocks of the Pyeongan Supergroup, Korea. Sediment Geol 149(4):219–235. https://doi.org/10.1016/S0037-0738(01)00174-9

Liritzis I, Bednarik R, Polymeris G, Iliopoulos I, Zacharias N, Kumar G, Vafiadou A, Bratitsi M (2019) Daraki-Chattan rock art constrained OSL chronology and multianalytical techniques: a first pilot investigation. J Cult Herit 37:29–43. https://doi.org/10.1016/j.culher.2018.09.018

Maravelis AG, Catuneanu O, Nordsvan A, Landenberger B, Zelilidis A (2018) Interplay of tectonism and eustasy during the Early Permian icehouse: Southern Sydney Basin, southeast Australia. Geol J 53:1372–1403

Maravelis AG, Makrodimitras G, Zelilidis A (2012) Hydrocarbon prospectivity in Western Greece. Oil Gas Eur J 38:84–89

Maravelis AG, Offler R, Pantopoulos G, Collins WJ (2021) Provenance and tectonic setting of the Early Permian sedimentary succession in the southern edge of the Sydney Basin, eastern Australia. Geol J 56:2258–2276

Maravelis AG, Pantopoulos G, Tserolas P, Zelilidis A (2015) Accretionary prism-forearc interactions as reflected in the sedimentary fill of southern Thrace Basin (Lemnos Island, NE Greece). Int J Earth Sci 104(4):1039–1060. https://doi.org/10.1007/s00531-014-1130-6

Maravelis AG, Pantopoulos G, Tserolas P, Zelilidis A (2017) Reply to comment by Caracciolo et al. on: Maravelis et al. 2015. "Accretionary prism-forearc interactions as reflected in the sedimentary fill of southern Thrace Basin (Lemnos Island, NE Greece)". Int J Earth Sci 106:389–394

Martins-Neto M, Catuneanu O (2010) Rift sequence stratigraphy. J Mar Pet Geol 27:247–253

McLennan J M (1981) The Cretaceous-Tertiary rocks ofAvoca, Oxford and Burnt Hill, central Canterbury.Unpublished M.Sc. thesis lodged in the Library,University of Canterbury, Christchurch, NewZealand

McLennan SM (1989) Rare earth elements in sedimentary rocks: influence of provenance and sedimentary process. Rev Mineral 21:169–200

McLennan SM, Hemming S, McDaniel DK, Hanson GN (1993) Geochemical approaches to sedimentation, provenance, and tectonics. In: Johnsson MJ, Basu A (eds) Processes controlling the composition of clastic sediments. Geological Society of America Special Paper, pp 21–40. https://doi.org/10.1130/SPE284-p21

McLennan SM, Taylor SR, McCulloch MT, Maynard JB (1990) Geochemical and Nd–Sr isotopic composition of deep-sea turbidites: crustal evolution and plate tectonic associations. Geochim Cosmochim Acta 54:2015–2050. https://doi.org/10.1016/0016-7037(90)90269-Q

McManus J, Francois R, Gherardi JM, Keigwin LD, Brown-Leger S (2004) Collapse and rapid resumption of Atlantic meridional circulation linked to deglacial climate changes. Nature 428(6985):834–837. https://doi.org/10.1038/nature02494

Melehan S, Botziolis C, Maravelis AG, Catuneanu O, Ruming K, Holmes E, Collins WJ (2021) Sedimentology and stratigraphy of an Upper Permian sedimentary succession: Northern Sydney Basin, Southeastern Australia. Geosciences 11:273. https://doi.org/10.3390/geosciences11070273

Miller MM, Saleeby JB (1995) U-Pb geochronology of detrital zircon from Upper Jurassic synorogenic turbidites, Galice Formation, and related rocks, western Klamath Mountains: Correlation and Klamath Mountains provenance. J Geophys Res 100(B9):18045–18058. https://doi.org/10.1029/95JB00761

Mountrakis D (1985) The geology of Greece. University Studio Press, p 207

Muttoni G, Carcano C, Garzanti E, Ghielmi M, Piccin A, Pini R, Rogledi S, Sciunnach D (2003) Onset of major Pleistocene glaciations in the Alps. Geology 31:989–992. https://doi.org/10.1130/G19445.1

Nagel S, Castelltort S, Garzanti E, Lin AT, Willett SD, Mouthereau F, Limonta M, Adatte T (2014) Provenance evolution during arc–continent collision: Sedimentary petrography of Miocene to Pleistocene sediments in the western foreland basin of Taiwan. Journal of Sedimentary Research, 84(7), 513– 528. https://doi.org/10.2110/jsr.2014.44

Najman Y, Appel E, Boudagher-Fadel M, Bown P, Carter A, Garzanti E, Parrish R (2010) Timing of India-Asia collision: geological, biostratigraphic, and palaeomagnetic constraints. J Geophys Res Solid Earth 115:B12416

Najman Y, Garzanti E (2000) Reconstructing early Himalayan tectonic evolution and paleogeography from Tertiary foreland basin sedimentary rocks, northern India. Geol Soc Am Bull 112:435–449. https://doi.org/10.1130/0016-7606(2000)112<0435:REHTEA>2.3.CO;2

Najman Y, Garzanti E, Pringle MS, Bickle M, Stix J, Khan I (2003) Early-Middle Miocene paleodrainage and tectonics in the Pakistan Himalaya. Geol Soc Am Bull 115:1265–1277. https://doi.org/10.1130/B25165.1

Nance RD, Murphy JB, Santosh M (2014) The supercontinent cycle: a retrospective essay. Gondwana Res 25:4–29

Nance WB, Taylor SR (1976) Rare earth element patterns and crustal evolution—I. Australian post-archean sedimentary rocks. Geochim Cosmochim Acta 40:1539–1551.https://doi.org/10.1016/0016-7037(76)90093-4

Nathan S (1976) Geochemistry of the Greenland Group (early Ordovician), New Zealand N.Z. J. Geol. Geophys. 19:683–706. https://doi.org/10.1080/00288306.1976.10426314

Nesbitt HW, Fedo CM, Young GM (1997) Quartz and feldspar stability, steady and non-steady-state weathering, and petrogenesis of siliciclastic sands and muds. J Geol 105(2):173–192

Nesbitt HW, Markovics G, Price RC (1980) Chemical processes affecting alkalis and alkaline earths during continental weathering. Geochim Cosmochim Acta 44:1659–1666

Nesbitt HW, Young GM (1982) Early Proterozoic climates and plate motions inferred from major element chemistry of lutites. Nature 299:715–717. https://doi.org/10.1038/299715a0

Nesbitt HW, Young GM (1984) Prediction of some weathering trends of plutonic and volcanic rocks based on thermodynamic and kinetic considerations. Geochim Cosmochim Acta 48:1523–1534. https://doi.org/10.1016/0016-7037(84)90408-3

Neuser RD, Richter DK, Vollbrecht A (1989) Natural quartz with brown-violet cathodoluminescence – genetic aspects evident from spectral analysis. Zbl Geol Palaont Teil I 1988:919–930

Papanikolaou D (2009) Timing of tectonic emplacement of the ophiolites and terrane paleogeography in the Hellenides. Lithos 108(1-4):262–280. https://doi.org/10.1016/j.lithos.2008.08.003

Pavlides SB, Zouros NC, Chatzipetros AA, Kostopoulos DS, Mountrakis DM (1995) The 13 May 1995 Western Macedonia, Greece (Kozani-Grevena) earthquake; preliminary results. Terra Nova 7:544–549
Pavlopoulos A (1983) Contribution to the geological investigation of Makrynoros flysch deposits, Akarnania. PhD, thesis,Aristotle University of Thessaloniki
Pearce JA (1982) Trace element characteristics of lavas from destructive plate boundaries. In: Thorpe RS (ed) Andesites: orogenic andesites and related rocks. John Wiley and Sons, pp 252–548
Pearce JA, Lippard SJ, Roberts S (1984) Characteristics and tectonic significance of suprasubduction zone ophiolites. In: Kokelaar B, Howells MF (eds) Marginal Basin Geology, vol 16. Geological Society of London, Special Publication, pp 77–94
Pe-Piper G (1982) Geochemistry, tectonic setting and metamorphism of the mid-Triassic volcanic rocks of Greece. Tectonophysics 85:253–272. https://doi.org/10.1016/0040-1951(82)90105-6
Pe-Piper G, Matarangas D, Jacobshagen V (1996) The Mesozoic metavolcanics rocks of Alonnisos and Kyra Panagia islands, Sporades, Greece. N Jb Miner Mh 6:251–263
Pe-Piper G, Panagos AG (1989) Geochemical characteristics of the Triassic volcanic rocks of Evia: petrogenetic and tectonic implications. Ofioliti 14:33–50
Pe-Piper G, Tsikouras B, Hatzipanagiotou K (2004) Evolution of boninites and island-arc tholeiites in the Pindos Ophiolite, Greece. Geol Mag 141(4):455–469. Cambridge University Press. https://doi.org/10.1017/S0016756804009215
Piper DJW (2006) Sedimentology and tectonic setting of the Pindos Flysch of the Peloponnese, Greece. In: Robertson AHF, Mountrakis D (eds) Tectonic Development of the Eastern Mediterranean Region, vol 260. Geological Society, London, Special Publications, pp 493–505. https://doi.org/10.1144/GSL.SP.2006.260.01.20
Piper DJW, Panagos G, Pe-Piper G (1978) Conglomeratic Miocene flysch, western Greece. J Sediment Res 48:117–126. https://doi.org/10.1306/212F740A-2B24-11D7-8648000102C1865D
Pomoni-Papaioannou F (1994) Palaeogeographic evolution of the Parnassus-Ghiona carbonate platform in the interval Late Maastrichtian-Paleocene, Greece. Geologie Mediterranee, XXI 3-4:153–154
Purevjav N, Roser B (2013) Geochemistry of Silurian-Carboniferous sedimentary rocks of the Ulaanbaatar terrane, Hangay-Hentey belt, central Mongolia: provenance, paleoweathering, tectonic setting, and relationship with the neighbouring Tsetserleg terrane. Chemie der Erde - Geochem 73:481–493. https://doi.org/10.1016/j.chemer.2013.03.003
Qayyum M, Niem AR, Lawrence RD (2001) Detrital modes and provenance of the Paleogene Khojak Formation in Pakistan: implications for early Himalayan orogeny and unroofing. Geol Soc Am Bull 113(3):320–332. https://doi.org/10.1130/0016-7606(2001)113<0320:dmapot>2.0.co;2
Ramseyer K, Baumann J, Matter A, Mullis J (1988) Cathodoluminescence colours of α-quartz. Mineral Mag 52(368):669–677
Ricou LE (1994) Tethys reconstructed: plates continental fragments and their boundaries since 260 Ma from Central America to South-Eastern Asia. Geodin Acta 7:169–218. https://doi.org/10.1080/09853111.1994.11105266
Robertson AHF (2004) Development of concepts concerning the genesis and emplacement of tethyan ophiolites in the Eastern Mediterranean and Oman Regions. Earth Sci Rev 66:331–387. https://doi.org/10.1016/j.earscirev.2004.01.005
Robertson AHF, Clift PD, Degnan PJ, Jones G (1991) Palaeogeographic and palaeotectonic evolution of the Eastern Mediterranean Neotethys. Palaeogeogr Palaeoclimatol Palaeoecol 87:289–343. https://doi.org/10.1016/0031-0182(91)90140-M
Roddaz M, Viers J, Brusset S, Baby P, Boucayrand C, Hérail G (2006) Controls on weathering and provenance in the Amazonian foreland basin: insights from major and trace element geochemistry of Neogene Amazonian sediments. Chem Geol 226(1–2):31–65
Rollinson HR (1993) Using geochemical data: evaluation, presentation, interpretation. Longman Scientific and Technical, Harlow, Essex, England: New York
Ryan KM, Williams DM (2007) Testing the reliability of discrimination diagrams for determining the tectonic depositional environment of ancient sedimentary basins. Chem Geol 242:103–125
Sagripanti L, Bottesi G, Kietzmann D, Folguera A, Ramos V (2012) Mountain building processes at the orogenic front. A study of the unroofing in Neogene foreland sequence (37°S). Andean Geol 39(2):201–219
Schieber J (1992) A combined petrographical-geochemical provenance study of the Newland formation, Mid-Proterozoic of Montana. Geol Mag 129:223–237. https://doi.org/10.1017/S0016756800008293
Schwab FL (1981) Evolution of the Western Continental Margin, French-Italian Alps: sandstone mineralogy as an index of plate tectonic setting. J Geol 89(3):349–368. https://doi.org/10.1086/628596
Sharp IR, Robertson AHF (2006) Tectonic-sedimentary evolution of the western margin of the Mesozoic Vardar Ocean: evidence from the Pelagonian and Almopias zones, northern Greece. Geol Soc, Lon, Spec Publ 260(1):373–412. https://doi.org/10.1144/gsl.sp.2006.260.01.16
Sinclair HD, Allen PA (1992) Vertical versus horizontal motions in the Alpine orogenic wedge: stratigraphic response in the foreland basin. Basin Res 4(3-4):215–232. https://doi.org/10.1111/j.1365-2117.1992.tb00046.x
Sippel RF (1965) Simple device for luminescence petrography. Rev Scient Intr 36:556–558. https://doi.org/10.1063/1.1719391
Sippel RF (1968) Sandstone petrology, evidence from luminescence petrography. J Sediment Petrol 38:530–554. https://doi.org/10.1306/74D719DD-2B21-11D7-8648000102C1865D
Skourlis K, Doutsos T (2003) The Pindos Fold-and-thrust belt (Greece): inversion kinematics of a passive continental margin. Int J Earth Sci 92(6):891–903. https://doi.org/10.1007/s00531-003-0365-4
Smith WHF (1993) On the accuracy of digital bathymetric data. J Geophys Res 98(B6):9591–9603. https://doi.org/10.1029/93JB00716
Smith AG, Hynes AJ, Menzies M, Nisbet EG, Price I, Welland MJP, Ferrière J (1975) The stratigraphy of the Othris mountains, eastern central Greece: a deformed Mesozoic continental margin sequence: Eclogae Geol 68:463-481. Helv
Smith AG, Moores EN (1974) Hellenides, in Spencer-Verlag. Mesozoic and Cenozoic orogenic belts. Geological Society of London Special Publication 4. p. 159-185
Smith AG, Woodcock NH, Naylor MA (1979) The structural evolution of a Mesozoic continental margin, Othris Mountains, Greece. J Geol Soc 136:589–601
Sotiropoulos S, Kamberis E, Triantaphyllou MV, Doutsos T (2003) Thrust sequences in the central part of the External Hellenides. Geol Mag 140:661–668. https://doi.org/10.1017/S0016756803008367
Stampfli GM (1996) Tire Intra-Alpine terrain: a Paleotethyan remnant in the Alpine Variscides. Eclogae Geol Helv 89:1342
Stampfli GM, Mosar J, De Bono A, Vavassis I (1998) Late Paleozoic, Early Mesozoic plate tectonics of the Western Tethys. Bull Geol Soc Greece 32(1):113–120
Tawfik HA, Salah MK, Maejima W, Armstrong-Altrin JS, Abdel-Hameed AT, Ghandour IM (2017) Petrography and geochemistry of the Lower Miocene Moghra sandstones, Qattara Depression, north Western Desert, Egypt. Geol J 53:1938–1953. https://doi.org/10.1002/gj.3025

Taylor SR, McLennan SM (1985) The Continental Crust: Its Composition and Evolution, Blackwell, Oxford, p. 312.
Taylor SR, McLennan SM (1995) The geochemical evolution of the continental crust. Rev Geophys 33:241–265
Tortosa A, Palomares M, Arribas J (1991) Quartz grain types in Holocene deposits from the Spanish Central System: some problems in provenance analysis. Geol Soc Lond 57:47–54. https://doi.org/10.1144/GSL.SP.1991.057.01.05
Tserolas P, Maravelis AG, Tsochandaris N, Pasadakis N, Zelilidis A (2019) Organic geochemistry of the Upper Miocene-Lower Pliocene sedimentary rocks in the Hellenic Fold and Thrust Belt, NW Corfu Island, Ionian Sea, NW Greece. Mar Pet Geol 106:17–29. https://doi.org/10.1016/j.marpetgeo.2019.04.033
Underhill J (1988) Triassic evaporites and Plio-Quaternary diapirism in Western Greece. J Geol Soc London 145:209–282. https://doi.org/10.1144/gsjgs.145.2.0269
Velić J, Malvić T, Cvetković M, Velić I (2015) Stratigraphy and petroleum geology of the Croatian part of the Adriaticbasin. J Pet Geol 38(3):281–300. https://doi.org/10.1111/jpg.12611
Verma SP, Armstrong-Altrin JS (2013) New multi-dimensional diagrams for tectonic discrimination of siliciclastic sediments and their application to Precambrian basins. Chem Geol 355:117–133. https://doi.org/10.1016/j.chemgeo.2013.07.014
Vital H, Stattegger K (2000) Sediment dynamics in the lowermost Amazon. J Coast Res 16(2):316–28. JSTOR, http://www.jstor.org/stable/4300040.
Von-Eynatten H, Barceló-Vidal C, Pawlowsky-Glahn V (2003) Composition and discrimination of sandstones: a statistical evaluation of different analytical methods. J Sediment Res 73:47–57. https://doi.org/10.1306/070102730047
Wagreich M, Pavlopoulos A, Faupl P, Migiros G (1996) Age and significance of Upper Cretaceous siliciclastic turbidites in the central Pindos Mountains, Greece. Geol Mag 133(3):325–331
Weaver CE (1989) Clays, muds and shales. Dev Sedimentol 44:1–5
Weislogel AL, Graham SA, Chang EZ, Wooden JL, Gehrels GE, Yang H (2006) Detrital zircon provenance of the Late Triassic Songpan-Ganzi complex: sedimentary record of collision of the North and South China blocks. Geology 34:97–100
White AF, Brantley SL (1995) Chemical weathering rates of silicate minerals. Mineralogical Society of America, Washington, D.C.
White NM, Pringle M, Garzanti E, Bickle M, Najman Y, Chapman H, Friend P (2002) Constraints on the exhumation and erosion of the High Himalayan Slab, NW India, from foreland basin deposits. Earth Planet Sci Lett 195:29–44. https://doi.org/10.1016/S0012-821X(01)00565-9
Wronkiewicz DJ, Condie KC (1990) Geochemistry and mineralogy of sediments from the Ventersdorp and Transvaal Supergroups, South Africa: Cratonic evolution during the early Proterozoic. Geochim Cosmochim Acta 54(2):343–354. https://doi.org/10.1016/0016-7037(90)90323-D
Xypolias P, Doutsos T (2000) Kinematics of rock flow in a crustal scale shear zone: implication for the orogenic evolution of the SW Hellenides. Geol Mag 137:81–96. https://doi.org/10.1017/S0016756800003496
Zaid SM, Gahtani FA (2015) Provenance, diagenesis, tectonic setting, and geochemistry of Hawkesbury sandstone (Middle Triassic), southern Sydney Basin, Australia. Turk J Earth Sci 24:72–98. https://doi.org/10.3906/yer-1407-5
Zelilidis A, Maravelis AG (2015) Introduction to the thematic issue: Adriatic and Ionian Seas: proven petroleum systems and future prospects. J Pet Geol 38:247–254. https://doi.org/10.1111/jpg.12609
Zelilidis A, Maravelis AG, Tserolas P, Konstantopoulos PA (2015) An overview of the Petroleum systems in the Ionian zone, onshore NW Greece and Albania. J Petr Geol 38(3):331–347. https://doi.org/10.1111/jpg.12614
Zelilidis A, Piper DJW, Vakalas I, Avramidis P, Getsos K (2003) Oil and gas plays in Albania: do equivalent plays exist in Greece? J Pet Geol 26:29–48. https://doi.org/10.1111/j.1747-5457.2003.tb00016.x
Zelilidis A, Vakalas I, Barkooky A, Darwish M, Tewfik N (2008) Impact of transfer faults and intrabasinal highs in basin evolution and sedimentation processes: application to potential hydrocarbon fields development. Adv Sci Lett 1:1–10. https://doi.org/10.1166/asl.2008.010
Zimmermann U, Spalletti LA (2009) Provenance of the lower Paleozoic Balcarce Formation (Tandilia System, Buenos Aires Province, Argentina): implications for paleogeographic reconstructions of SW Gondwana. Sediment Geol 219:7–23. https://doi.org/10.1016/j.sedgeo.2009.02.002
Zinkernagel U (1978) Cathodoluminescence of quartz and its application to sandstone petrology. Contrib Sediment Geol 8:69
Zoumpouli E, Maravelis AG, Iliopoulos G, Botziolis C, Zygouri V, Zelilidis A (2022) Re-Evaluation of the Ionian Basin Evolution during the Late Cretaceous to Eocene (Aetoloakarnania Area, Western Greece). Geosciences 12(3):106. https://doi.org/10.3390/geosciences12030106
Zygouri V, Maravelis AG, Zoumpouli E, Botziolis C, Zelilidis A (2021) Thrust and strike-slip fault control, in the late Eocene to Miocene, of Pindos foreland basin evolution: SE Aitoloakarnania area, western Greece. GeoKarlsruhe 2021. https://doi.org/10.13140/RG.2.2.21886.51528